JOURNAL OF GEOPHYSICAL RESEARCH, VOL. 92, NO. A2, PAGES 1075–1092, FEBRUARY 1, 1987

Characteristics of Electron Velocity Distribution Functions in the Solar Wind Derived From the Helios Plasma Experiment

W. G. PILIPP,[1] H. MIGGENRIEDER,[2] M. D. MONTGOMERY,[3] K.-H. MÜHLHÄUSER,[1] H. ROSENBAUER,[4] AND R. SCHWENN[4]

The shapes of three typical examples of electron distribution functions, which have been observed by Helios 2 in the solar wind, are analyzed and compared with theoretical predictions. We have considered a distribution function with a "narrow strahl" (narrow beam), which is extremely anisotropic and skewed with respect to the magnetic field direction at particle energies above 100 eV, a distribution function with a "broad strahl" (broad beam), which is less anisotropic and skewed, and finally a nearly isotropic distribution function which, however, shows a slight bidirectional anisotropy. The main results are as follows: (1) For each distribution function we may discern a "break," i.e., a sudden change in the slope of the distribution function, separating the "core" at lower energies from the "halo" at larger energies. For the anisotropic distributions a significant break is observed in velocity directions opposite to the strahl and perpendicular to it but not along the strahl. Here the energy of the break (breakpoint energy) may be determined both by the interplanetary electrostatic potential and by collisions. In contrast, for the nearly isotropic distribution function, a significant break is observed for all velocity directions, and the breakpoint energy may be determined by collisions only. (2) The strahl observed at larger energies in the anisotropic distribution functions can be qualitatively explained by existing theoretical approaches describing the propagation of electrons in the solar wind. However, at least for the distribution function with the broad strahl as well as for the nearly isotropic distribution function, the halo electrons should be scattered by unknown anomalous scattering processes, which do not show a strong energy dependence. (3) For the anisotropic distribution functions we find a velocity shift between the peak of each distribution function and the solar wind bulk velocity, which is typically 100 km s^{-1} to 300 km s^{-1}. This shift is drastically reduced compared to the shift predicted by exospheric theory, indicating strong frictional processes between electrons and ions. However the results do not settle the question whether this friction is provided by the combined action of wave-particle interactions and Coulomb collisions or by Coulomb collisions only. For the nearly isotropic distribution function this shift is probably not significantly different from zero. In this case it may be determined by some anomalous processes and/or trapping in closed magnetic field structures. (4) For the anisotropic distribution functions the heat flux is carried mainly by the strahl. For the nearly isotropic distribution function most of the heat flux is carried by the core electrons. For this distribution, part of the halo electrons carry heat flux in the opposite direction, and the total heat flux is probably not significantly different from zero. (5) The pitch angle distribution in the energy regime of the halo may provide some indications for the global structure of the magnetic field.

1. INTRODUCTION

The study of electrons in the solar wind is interesting for several reasons:It may provide some insight into the mechanisms controlling the heat flux in a dilute hot extraterrestrial plasma. (In the solar wind the electrons carry the largest part of the total heat flux.) The electron temperature observed in the solar wind may represent to some extent a signature of the temperature in the solar corona from where the electrons emanate. The more energetic electrons may trace the field lines of the interplanetary magnetic field without strong scattering and thus may serve as a probe for the global structure of the magnetic field. Finally, details of the electron distribution functions are important for resonant microinstabilities which may contribute at least partly to the high frequency turbulence of the solar wind plasma.

For the last 20 years or so, various electron measurements have been performed aboard many spacecraft near the orbit of earth as well as aboard space probes traveling deep into the interplanetary space. The early observations have already shown that the solar wind electrons are not in thermodynamic equilibrium and that they are not thermally coupled to the protons. Velocity distributions for solar wind electrons were determined for the first time by *Montgomery et al.* [1968] from VELA measurements. Two-dimensional reduced distribution functions integrated over the polar angle of the spacecraft were obtained. These distributions could be fitted fairly well by Maxwellians at energies below about 50 eV but were significantly enhanced above these fits at larger energies. In addition, the distribution functions were found to be anisotropic and skewed with respect to the magnetic field direction with a temperature $T_{e\parallel}$ (parallel to the magnetic field) larger than the temperature $T_{e\perp}$ (perpendicular to it) by a factor of 1.1 or 1.2 and a heat flux along the magnetic field ranging from 5×10^{-3} to 2×10^{-2} erg cm^{-2} s^{-1}. The electron temperatures were observed to vary typically between 0.7×10^5 K and 2×10^5 K, fluctuating much less than the proton temperatures. More detailed investigations by *Montgomery* [1972*a*, *b*] largely confirmed these results and provided indications that the observed heat flux cannot be described by the classical transport theory of *Spitzer and Härm* [1953]. For the electron temperatures,

[1]Institut für extraterrestrische Physik, Max-Planck-Institut für Physik und Astrophysik, Garching, Federal Republic of Germany.
[2]Bayerisches Staatsministerium für Landesentwicklung und Umweltfragen, Munich, Federal Republic of Germany.
[3]Maxwell Laboratories, Inc., San Diego, California.
[4]Max-Planck-Institut für Aeronomie, Katlenburg-Lindau, Federal Republic of Germany.

Paper number 5A8095.
0148-0227/87/005A-8095$05.00

similar results have been reported from various other spacecraft measurements near the orbit of earth by *Formisano* [1969], *Serbu* [1972], *Feldman et al.* [1973], and *Scudder et al.* [1973]. *Ogilvie et al.* [1971] derived from OGO 5 measurements the differential electron heat flux as a function of the pitch angle relative to the magnetic field direction and of an upper limit E_u for the electron energy which has been varied up to 9.9 keV. They showed that the heat flux was always directed along the magnetic field away from the sun (as far as the solar wind was not disturbed by the earth's bow shock) and was often strongly colliminated along the magnetic field direction. In addition, it was observed to be lower than 10^{-2} erg cm^{-2} s^{-1} for electrons with energies below 300 eV (i.e., for $E_u \leq 300$ eV) in rough agreement with the VELA observations. However, Ogilvie et al. found also that the heat flux can increase to much larger values for increasing E_u if an anomalous "tail" of energetic electrons is present due to transient electrons which are emitted from time to time from the sun [see also *Scudder,* 1972].

The analysis of the measurements aboard the earth-orbiting IMP spacecraft by *Feldman et al.* [1974, 1975, 1978] yielded additional details of the electron distribution functions and showed that the electron properties are correlated with the plasma stream structures of the solar wind. For these investigations each electron distribution function was described by a superposition of two components: the core or the cool component and the halo or the hot component. The core was fitted to a bi-Maxwellian multiplied by a heat flux term, and the halo to a bi-Maxwellian. The core, comprising the electrons with energies below 50 eV to 100 eV (and thus representing the bulk of the electrons), turned out to be rather isotropic or only moderately anisotropic. The halo, representing the electrons at larger energies (typically 5% of the total electron number), was often found to be appreciably anisotropic. In addition, the core and the halo were found to be shifted relative to each other along the magnetic field. The core is shifted in the solar direction and the halo in the antisolar direction relative to the solar wind bulk velocity. *Feldman et al.* [1975, 1978] also found that the core and halo temperatures vary generally together across the stream structures. In high-speed streams the temperatures are usually depressed as compared to the slow solar wind. The thermal anisotropies of the core and the halo and the velocity shift between these two components proved to be much larger in high-speed streams than in the slow solar wind.

Electron velocity distribution functions with increased resolution in velocity space have been obtained from measurements of the Helios electron instrument. For many of these distribution functions, *Rosenbauer et al.* [1976, 1977] detected an additional nonthermal feature which has been termed "strahl" (beam), which denotes an extreme anisotropy and skewness with respect to the magnetic field direction in the energy regime of the halo. This feature implies that most halo electrons stream away from the sun along the magnetic field with small pitch angles. The strahl, which is responsible for the strong temperature anisotropy of the halo as well as the velocity shift between the core and the halo, has been found predominantly in high-speed streams [*Rosenbauer et al.,* 1977]. *Feldman et al.* [1978, 1982] found that the angular width of the strahl correlates with the plasma stream structure, being smallest in high-speed streams where the angular width has been found to decrease with particle energy down to 15° or 12° for energies of 247 eV.

Besides these correlations of electron data with the plasma streams, there have been preliminary indications from Helios data [*Pilipp et al.,* 1981] that the thermal electron properties as well as the occurrence of the strahl are more strongly correlated with the sector structure of the magnetic field than with the solar wind bulk velocity. In particular, a strong strahl has usually been found within the interior of magnetic sectors, whereas at sector boundaries the strahl is missing.

In addition, in some sporadic cases, anisotropic electron distribution functions with symmetric bidirectional streaming of halo electrons along the magnetic field were observed, which were interpreted to indicate closed magnetic field loops. *Montgomery et al.* [1974] found from VELA and IMP observations distinct depressions of electron temperatures correlated with the occurrence of a component of higher energy electrons streaming symmetrically in both directions along the magnetic field after shock waves. They interpreted their observations as likely to be due to the passage of closed magnetic field structures following flare-induced shock waves. Also *Temnyi and Vaisberg* [1979] have observed from Prognoz 7 data and *Bame et al.* [1981] from ISEE 3 data electron distribution functions with a symmetric bidirectional streaming of the halo electrons along the magnetic field in solar wind regions following shock waves, again indicating closed magnetic field structures. A sunward directed strahl, implying a preferred motion of halo electrons with small pitch angles toward the sun, was reported by *Ogilvie and Scudder* [1981]. This feature was observed by Mariner 10 in few cases, early in the encounter of the spacecraft with a high-speed stream. The angular width of sunward directed strahl was found to decrease with increasing particle energy down to about 13° at an energy of 350 eV. Since the electron spectrometer aboard Mariner 10 observed only electrons in motion toward the sun, the measurements did not show whether this strahl was the sunward part of a symmetric bidirectional streaming or whether it was due to a mainly unidirectional streaming of energetic electrons toward the sun. Ogilvie and Scudder offered two explanations for these observations: (1) The electrons were observed in a kinked magnetic field configuration directing the strahl locally toward the sun. (2) The electrons scattered back toward the sun were focused into a strahl by moving from a compression region with higher magnetic field strength into a region of lower magnetic field strength before it.

Information on the processes affecting the propagation of electrons in the solar wind should come also from the observed variation of electron parameters with distance from the sun [*Rosenbauer et al.,* 1977; *Ogilvie and Scudder,* 1978; *Sittler and Scudder,* 1980; *Sittler et al.,* 1981; *Feldman et al.,* 1979*a*]. However, determination of radial gradients is difficult because the solar wind is strongly structured in space and time.

It is the purpose of the present paper and of *Pilipp et al.* [this issue (*a*, *b*)] and *Pilipp* [1983] to reexamine and to extend earlier investigations about the structural details of electron distribution functions as well as variations of electron properties in the solar wind. The results presented here are derived from measurements which have been made aboard the Helios probes at distances between 0.3 AU and 1 AU from the sun. The methods of data analysis for these electron measurements have been described in much detail in the report by *Pilipp et al.* [1984] and are outlined in section

2 of the present paper. The magnetic field data used for our analysis have been provided from the Technische Universität (TU) Braunschweig magnetometer experiment [*Musmann et al.*, 1975, 1977; *Neubauer et al.*, 1977].

For the present paper we concentrate on the first 107 days of the Helios 2 mission from January 18 to May 3, 1976, right before solar minimum. This period is particularly appropriate for our analysis. Here we have the best data coverage, and the Helios 2 probe moved from the orbit of earth toward perihelion and somewhat back again, thus covering the whole distance range between 0.29 and 1 AU. In addition, long-lived high-speed streams were still present, allowing investigation of relatively stationary and pure high- and low-speed streams [*Sheeley and Harvey*, 1978]. The status of the corona and the interplanetary plasma during that period, as well as associated proton and alpha particle distributions, has been described in more detail by *Marsch et al.* [1982*a*, *b*].

2. Experimental Characteristics and Data Analysis Procedure

2.1. *Basic Instrumental Facts*

The Helios 1 spacecraft was launched on December 10, 1974, into an ecliptic orbit around the sun. The perihelion at 0.31 AU was reached for the first time on March 15, 1975. Helios 2 was launched on January 15, 1976, into a similar orbit, performing its first perihelion passage at 0.29 on April 17, 1976. Both Helios spacecraft are nearly identical, being shaped like a spool. Except for the radial booms and the antenna the probes are nearly rotationally symmetric about their spin axes, continuously oriented perpendicular to the ecliptic plane, and are symmetric with respect to their equatorial planes. For general information about the Helios mission, see *Porsche* [1975, 1977].

Solar wind electrons have been observed on both spacecraft with nearly identical electron analyzers, each employing a combination of plane and hemispherical plate electrostatic defectors, described by *Schwenn et al.* [1975] and *Rosenbauer et al.* [1977, 1981]. The apertures of the instruments are situated in the equatorial plane of each spacecraft. Their field of view is perpendicular to the spin axis, i.e., along the ecliptic plane, and perpendicular to the surface of the spacecraft. The electrons are analyzed with respect to their energy E in 32 energy channels. Sixteen energy channels are distributed between 0.004 eV and 15.5 eV (low energy mode), and 16 channels are distributed between 10.69 eV and 1658 eV (high energy mode). The energy resolution $\delta E/E$ is about 6%, and the channels of the high energy mode are logarithmically spaced with a factor of 1.4 for the energy ratio of neighboring energy channels.

The electrons are also analyzed with respect to their velocity directions by making use of the spacecraft rotation with a spin period of 1 s. For every satellite revolution the electron flux is measured in eight angular channels directed parallel to the ecliptic plane and spaced 45° apart at a fixed energy channel. The polar acceptance angle of the instrument is about 19° full width at half maximum (FWHM) centered on the ecliptic plane. The azimuthal acceptance angle is about 2° FWHM. But the electrons are counted within individual channels of measurement during a time interval of 78.06 ms for Helios 1 and 31.1 ms for Helios 2, corresponding to rotation angles of the probe of 28.1° and 11.2°, respectively. The integral azimuthal range for an individual channel of measurement is about 30° for Helios 1 and 13° for Helios 2. Thus the Helios electron instruments have a narrow angular field of view.

Depending on the experimental mode, one electron spectrum is formed by the count rates in the eight angular channels and either in all 32 energy channels of both energy modes or in the 16 energy channels of one energy mode only (high energy mode or low energy mode, alternatively). For the high bit rate (2048 bits/s) and the telemetry format usually used, one complete spectrum for each of the energy modes is obtained in 18 s or 16 s (depending on the experimental mode). The usual repetition time for the cycles of measurement is 40 s. For lower bit rates and/or different telemetry formats the time for obtaining one spectrum as well as the repetition time may be longer (for details, see *Rosenbauer et al.* [1981]).

2.2. *Corrections and Interpolations*

In order to find the correct electron distribution functions from the measurements one has to distinguish carefully between photoelectrons and solar wind electrons. In addition, since the spacecraft becomes electrically charged due to the emission of photoelectrons as well as to currents from solar wind electrons and ions, an electrostatic spacecraft potential is built up which accelerates or decelerates solar wind electrons before they enter the instrument. The observed electron velocities have to be corrected accordingly.

The spatial distributions of the electrostatic potential as well as space charges around the Helios probe have been discussed by *Rosenbauer* [1973]. Extensive calculations for these distributions have been done by *Voigt et al.* [1981] [see also *Isensee*, 1977; *Voigt et al.*, 1980; *Isensee and Maassberg*, 1981; *Maassberg and Isensee*, 1981]. From the results of these model calculations and also from the analysis of the measured electron spectra at low energies it seems that major disturbances by photoelectrons occur usually for energies below 5 eV. For energies above 10 eV the observed spectra should be merely due to solar wind electrons [*Voigt et al.*, 1981; *Rosenbauer et al.*, 1976]. Therefore, in order to be sure that the observed count rates used for our analysis are exclusively due to solar wind electrons without any admixture of photoelectrons, we have taken into account only electron observations above 10 eV; i.e., the distribution functions for solar wind electrons have been determined at the 16×8 grid points in velocity space corresponding to the channels of measurement of the high energy mode only. From the count rates in these channels of measurement we are able to infer the electron phase space density at the grid points in the plane of measurement parallel to the ecliptic plane, after correction for the postacceleration of the electrons by the spacecraft potential ϕ_{SC} (potential at the instrument). Here we have determined ϕ_{SC} in such a way that the resulting electron number density N_e and the electron bulk velocity $\mathbf{V}_e$ are in reasonable agreement with the proton number density N_p and proton bulk velocity $\mathbf{V}_p$, respectively, assuming quasi-neutrality and vanishing electric current (and neglecting the alpha particles). The spacecraft potential was found to vary typically from 5 V to -5 V and to be much more often positive than negative.

According to earlier measurements the low energy part (say below 50 eV) of the electron distribution functions can be fitted fairly well to a Maxwellian distribution [*Montgomery et al.*, 1968; *Feldman et al.*, 1975; *Ogilvie and Scudder*,

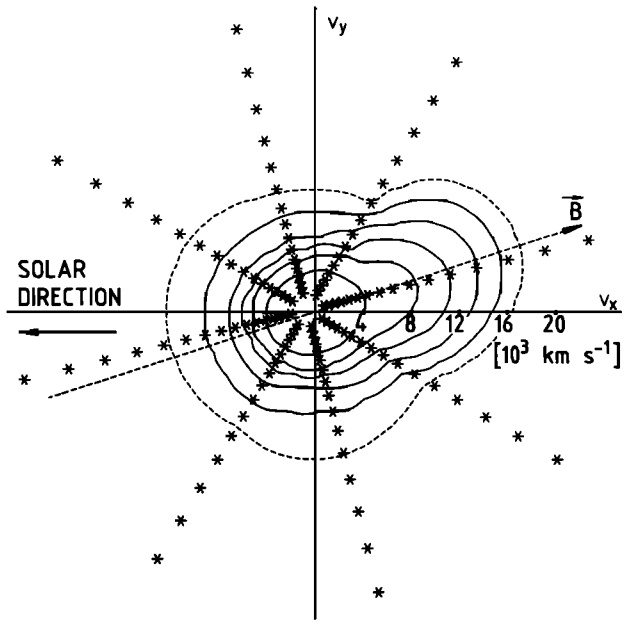

Fig. 1. A cut through an electron distribution function along the plane of measurement (parallel to the ecliptic plane) as observed during one cycle of measurement. The maximum of the phase space density is at the origin of the coordinate system (V_x, V_y), and the phase space density decreases with particle energy for each velocity direction. The phase space density is represented by contour lines that are logarithmically spaced and correspond to fractions 10^{-1}, 10^{-2}, $\cdots$, 10^{-6} of the maximum. The centers for the channels of measurement are indicated by asterisks. The magnetic field direction (averaged over the time of measurement) is very close to the plane of measurement (within 0.1°), and its projection onto this plane is indicated by the straight dashed line through the origin of the coordinate system.

1978]. We have used a bi-Maxwellian fit at low energies to extrapolate the phase density to energies below 10.69 eV (lowest energy channel of the high energy mode); i.e., we have supplemented our grid points by a point at zero energy where the phase space density is given by the bi-Maxwellian fit. For certain measurement modes the count rates of the lowest energy channel are missing for four angular channels. In this case we have used the bi-Maxwellian fit also for extrapolation of the phase density to these missing channels. Then we have interpolated the logarithm of phase space density at these grid points piecewise by biquadratic polynomials. Such an interpolation provides a continuous function describing the phase space density within the plane of measurement, which exactly reproduces a Maxwellian if the values for the phase space density at the grid points are taken from an assumed Maxwellian distribution.

Figure 1 shows an example of an electron distribution function which has been derived from Helios 2 measurements according to the method outlined above. The contour lines represent the phase space density in the plane of measurement parallel to the ecliptic plane and are logarithmically spaced corresponding to fractions 10^{-1}, 10^{-2}, $\cdots$, 10^{-6} of the maximum phase space density F_{Max}. The dashed contour line corresponds to count rates below 4 in at least one of the velocity directions along or perpendicular to the magnetic field. The coordinate system (V_x, V_y) is centered at the maximum of the distribution function with the V_x axis pointing radially away from the sun, the V_z axis (not shown) pointing to the north ecliptic and the V_y axis completing the right-handed coordinate system. The centers for the channels of measurement are indicated by asterisks, and the straight dashed line through the origin of the coordinate system indicates the projection of the magnetic field direction onto the ecliptic plane. The magnetic field is a16-s time average of the magnetic field data observed simultaneously by the TU Braunschweig magnetometer experiment [*Musmann et al.*, 1975, 1977]. For the distribution function shown here the magnetic field is parallel within 0.1° to the ecliptic plane so that the contour plot contains essentially all pitch angles with respect to the magnetic field direction. It can be seen that this distribution function shows a strong strahl as evidenced by the strong bulging of the contour lines along the magnetic field in antisolar direction for particle velocities well above 4×10^3 km s^{-1} or particle energies above 50 eV.

The phase space density within the plane of measurement is only a two-dimensional cut through the distribution functions of the electrons. However, in order to get the velocity moments the full three-dimensional distribution functions have to be known. These distribution functions may be constructed by rotation of the two-dimensional cuts about an axis parallel to the magnetic field direction, assuming that the electron distribution functions are gyrotropic about the magnetic field direction and provided that the magnetic field **B** is directed parallel to the plane of measurement, i.e., the ecliptic plane.

Since the gyroperiod of the electrons in the solar wind is very short (typically 10^{-3} to 10^{-2} s) compared to the time of measurement for one electron spectrum, we can assume the electron distributions to be gyrotropic about the magnetic field direction as seen from any frame of reference where the $\mathbf{E} \times \mathbf{B}$ drift vanishes. Here **E** is the electric field. (In fact, for the energy range considered here, the only significant drift should be the $\mathbf{E} \times \mathbf{B}$ drift, at least for usual solar wind conditions.) The solar wind rest frame is such a frame of reference. In this frame the peaks of the gyrotropic electron distribution functions could move at most along the magnetic field if each distribution function has only one distinct peak, as is practically always the case. Thus the electron distribution functions should also be gyrotropic in the frame of reference where the respective peak is at rest. Although in transport theories the distribution functions are usually considered in the center of mass frame, we consider the electron distribution functions mostly in the respective peak rest frame. The reason is that the peak of each distribution function can be determined more reliably (from the bi-Maxwellian core fit) than the bulk velocity.

In our analysis we consider the maxima of the bi-Maxwellian core fits to be the peaks of the electron distribution functions, where we neglect a possible motion of these peaks perpendicular to the ecliptic plane. In fact, the perpendicular velocity of the peaks should be very small compared to the average thermal electron velocity for two reasons: First, the velocity shift of these peaks relative to the solar wind bulk velocity is usually smaller than the solar wind bulk velocity and thus small compared to the average electron thermal velocity (see also next section), where the solar wind moves nearly parallel to the ecliptic plane. Second, we have analyzed usually only electron spectra with $|\varepsilon_B| \leq 10°$, where ε_B is the elevation angle of the magnetic field relative to the ecliptic plane so that the perpendicular component of the

velocity shift is smaller than the total shift by the factor sin 10° or less.

Generally, the magnetic field is not directed parallel to the ecliptic plane, so that rotation of the observed two-dimensional distribution functions about the axes parallel to the magnetic field and going through the respective peaks does not yield the entire three-dimensional distribution functions. Instead, each distribution function remains undefined within two cones, with the axes along the magnetic field in opposite directions and with the half angel ε_B. However, since we have usually analyzed only electron spectra with $|\varepsilon_B| \leq 10°$, the error introduced by extrapolation into these cones remains small anyway. We supplement the distribution functions by assuming that they are isotropic within these two cones. For each cone the phase space density is taken to be equal to the one found within the ecliptic plane at the corresponding particle energy and in the direction along the projection of the magnetic field.

From the derived distribution functions we can calculate the velocity moments, i.e., the electron number density N_e, the electron bulk velocity $\mathbf{V}_e$, the electron temperatures $T_{e\parallel}$ and $T_{e\perp}$ parallel and perpendicular to $\mathbf{B}$, respectively, and the heat flux vector $\mathbf{Q}_e$ directed along $\mathbf{B}$.

However, in contrast to the proton parameters, the electron velocity moments as derived from our analysis depend appreciably on the spacecraft potential, which is not known in advance. In particular, the derived electron number density N_e is a sensitive function of this unknown potential. As has been mentioned above, we have determined the spacecraft potential by assuming that the electron number density N_e and the electron bulk velocity $\mathbf{V}_e$ are in reasonable agreement with the proton number density N_p and the proton bulk velocity $\mathbf{V}_p$, respectively, assuming quasi-neutrality and zero current condition and neglecting alpha particles.

In fact, if not stated otherwise, the proton data N_p and $\mathbf{V}_p$ will be used as the solar wind density and bulk velocity. These data are given by the ion instrument I1a described by *Rosenbauer et al.* [1977]. The proton number density N_p as determined by the ion instrument is given within a maximum uncertainty of 20%, where the proton density was cross calibrated in orbit using the plasma wave instrument during the occurrence of plasma oscillations, the frequency of which is a function of density alone [*Gurnett and Anderson*, 1977]. The uncertainty for the proton bulk velocity $\mathbf{V}_p$ is less than 1% [*Marsch et al.*, 1982*a*].

The electron velocity moments, which are of major interest, are the electron temperatures $T_{e\parallel}$, $T_{e\perp}$ and the heat flux. The errors for these thermal electron properties are mainly due to remaining uncertainties in the determination of the spacecraft potential and due to finite resolution in phase space and in time. The errors for the electron temperatures are typically below 10%. The electron heat flux $Q = |\mathbf{Q}|$ (including a correction by the factor N_p/N_e in order to take advantage of the higher accuracy of proton density) may be uncertain up to a factor of 2. For most spectra the error in Q is below 50%.

2.3. *Improvement of Angular Resolution*

Since the strahl in the distribution functions for solar wind electrons is usually observed in only one angular channel (e.g., as in Figure 1), one can only determine an upper limit for the angular width of the strahl from a spectrum obtained in one cycle of measurement. This upper limit is given by the spacing of 45° between two neighboring angular channels. However, a much higher angular resolution can be achieved at the expense of time resolution if we employ a technique which has been introduced by *Ogilvie et al.* [1971] for analyzing their OGO 5 electron data. This technique exploits the fact that for a time-varying magnetic field the individual channels of measurement may belong to different pitch angles relative to the magnetic field direction in successive cycles of measurement.

As has been discussed above, we expect the electron distribution functions to be gyrotropic about the magnetic field direction as seen in a frame of reference moving with the peaks of the distributions. The magnetic field direction may change in time relative to the angular channels, but the electron distribution functions are postulated to remain stationary with respect to a polar coordinate system with the polar axis along the actual magnetic field direction and the origin fixed at the maximum of the distribution functions, at least for several cycles of measurement. Then we can combine the count rates observed at many different pitch angles during such a time interval to construct a distribution function with high angular resolution. This method is particularly appropriate for Helios 2 observations. Here the angular channels are shifted by 22.5° from one measurement cycle to the next one, which helps to improve coverage of the range of pitch angles even if the magnetic field direction varies only by a small amount. Taking into account the main sources for the limitation of angular resolution as discussed below, we conclude that at least for the Helios 2 results the angular width of a narrow strahl is resolved roughly within 10° to 15° degrees or better. For the Helios 1 results as shown in a companion paper [*Pilipp et al.*, this issue (*a*)] the angular width of the strahl may be resolved somewhat less accurately.

The angular resolution should be determined mainly by the following limitations:

1. One source of inaccuracy stems from the finite angular distance between neighboring channels of measurement in the pitch angle range from 0° to 180°. (Here the pitch angle of 0° corresponds to a particle velocity directed along the magnetic field away from the sun so that the strahl is usually at small pitch angles.) For most distribution functions with high angular resolution we have superimposed the data from 8 to 10 cycles of measurement. Then, for each energy channel, we have count rates at 64 to 80 different pitch angles (where each cycle of measurement contributes eight angular channels) so that the average angular distance between neighboring channels in the pitch angle range from 0° to 180° is less than 3°. Of course, the pitch angles are not equidistantly distributed. However, for the results presented in the present paper, the variability of the magnetic field direction was large enough to provide a fairly uniform coverage of data in the entire pitch angle regime (see also Figure 3). This holds true also for most of the results presented in the companion papers, besides a few exceptions where gaps up to 10° or 20° may occur in the pitch angle distributions.

2. Another inaccuracy limiting the angular resolution results from the fact that for each cycle of measurement the pitch angles are calculated from a 16-s time average magnetic field direction, averaged approximately over the time of 16 s to 18 s for obtaining an electron spectrum. Then the mag-

netic field direction actually occurring during the time of measurement for an individual channel may deviate from this averaged magnetic field direction. In order to confine the error for the calculated pitch angles due to this uncertainty of the magnetic field direction to less than about 10°, we have selected for our superposition only cycles of measurement where the mean square deviation of the magnetic field direction during each cycle is less than 8.6°.

3. Also the finite response width of each channel of measurement limits angular resolution, i.e., the polar acceptance angle of about 19° FWHM centered at the ecliptic plane and the integral azimuthal range of about 30° for Helios 1 and about 13° for Helios 2. From calculations similar to those derived by *Feldman et al.* [1978] it can be seen that the angular resolution of a narrow strahl is mainly limited by the finite azimuthal range width rather than by the polar acceptance angle if the magnetic field (and thus the strahl) is directed parallel to the ecliptic plane (i.e., the plane of measurement). Then the finite response of the instrument should limit resolution of a narrow strahl to 6.5° for Helios 2 and to 15° for Helios 1. For our procedure to construct distribution functions of high angular resolution we have selected only cycles of measurement where the magnetic field direction was parallel to the ecliptic plane within ±5°. Then we expect that the finite response of each channel of measurement limits angular resolution of a narrow strahl to less than 9° for Helios 2 and to less than 16° for Helios 1.

In order to resolve the angular width of a strahl still more accurately we have used the following procedure: We have represented the phase space density by a function depending on several free parameters, and then we have calculated from this function the count rates expected at the channels of measurement. The free parameters are then determined by a least squares fit of the calculated count rates to the observed count rates. More details of this procedure are described by *Pilipp et al.* [1984]. In this manner an angular resolution better than the instrumental response width may be obtained although an estimate of the remaining errors has not been derived.

Thus from this method we should be able to resolve a strahl with a much higher accuracy than the angular distance of 45° between neighboring angular channels, whereas the time resolution ranges from several minutes to a few hours depending on the interval of observation time for the superimposed electron spectra. For the results presented in our papers we use both types of electron distributions, with angular resolution of 45° but high time resolution (20 s or so) as described in section 2.2 and distribution functions with high angular resolution but poor time resolution.

3. Shapes of Individual Electron Distribution Functions

In this section we discuss details of typical distribution functions as they are usually observed in the solar wind in different stream structures. If not stated otherwise, we present the distributions in a frame of reference where the maximum of the respective distribution function is at rest. These frames of reference move nearly with the solar wind plasma, except for a shift δV_c between the phase space maxima and the solar wind bulk velocity which is smaller than the solar wind bulk velocity and thus small compared to the average electron thermal velocity (see discussion below).

The strahl, the most striking new feature in the distribution functions detected from Helios measurements, has proved to occur quite regularly in high-speed streams [*Rosenbauer et al.*, 1977; *Feldman et al.*, 1978]. However, distribution functions which are only moderately anisotropic or even nearly isotropic are also frequently observed in the solar wind. In Figure 2 we present three examples of electron distribution functions which have been derived with high angular resolution using the methods described in section 2.3. The three examples may be considered as typical in the sense that most electron distribution functions derived from the Helios measurements were found to be qualitatively similar to one of these examples. As will be detailed in a companion paper, the electron distribution functions as usually observed in the solar wind are strongly correlated with the sector structure of the interplanetary magnetic field [*Pilipp et al.*, this issue (*b*)]. The distribution function with the narrow strahl (Figure 2*a*) was observed at 0.3 AU in a high-speed stream embedded within the interior of a magnetic sector where the proton bulk velocity V_p was 691 km s^{-1}, the proton number density $N_p \approx 27$ cm^{-3}, and the proton temperature $T_p \approx 3.1 \times 10^5$ K. The moderately anisotropic distribution function with the broad strahl (Figure 2*b*) was observed at 0.7 AU in the trailing edge of a high-speed stream near but still outside a magnetic sector boundary with $V_p \approx 491$ km s^{-1}, $N_p \approx 6$ cm^{-3}, and $T_p \approx 1.3 \times 10^5$ K. Finally, the nearly isotropic distribution function (Figure 2*c*) was observed shortly afterward, again at 0.7 AU but right at a sector boundary with $V_p \approx 419$ km s^{-1}, $N_p \approx 16$ cm^{-3}, and $T_p \approx 0.7 \times 10^5$ K. These distribution functions are all gyrotropic according to the method of construction from measurements. The contour lines represent the phase space density within a plane of velocity space parallel to the magnetic field direction and going through the maximum of each distribution function. The coordinate system ($V_\parallel$, $V_\perp$) in each contour plot is centered at the maximum of the respective distribution function, and the positive $V_\parallel$ axis points along the magnetic field direction away from the sun. The distribution functions are monotonically decreasing with increasing particle velocity. The contour lines correspond to

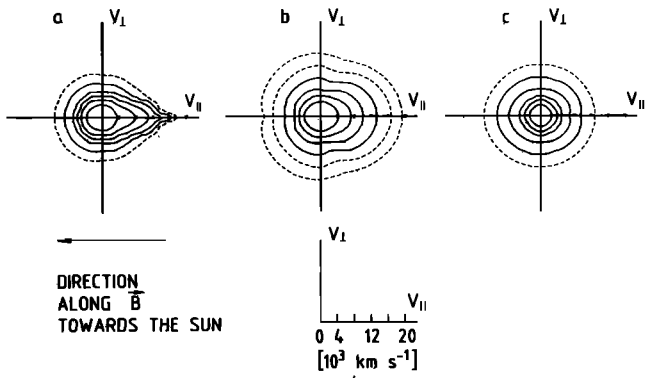

Fig. 2. Distribution functions with high angular resolution as constructed from measurements obtained during several cycles of measurement (see section 2.3). Each distribution function is represented by contour lines of phase space density in a plane of velocity space parallel to the magnetic field direction and going through the maximum of the respective distribution function. The maximum phase space density is at the origin of the coordinate system ($V_\parallel$, $V_\perp$), and the contour lines correspond to fractions 10^{-1}, 10^{-2}, ..., 10^{-6} of the maximum, respectively. Here we show three typical examples: a distribution function with a narrow strahl (Figure 2*a*), a distribution function with a broad strahl (Figure 2*b*), and a nearly isotropic distribution function (Figure 2*c*).

fractions 10^{-1}, 10^{-2}, $\cdots$, 10^{-6} of the respective maximum phase space density. (The dashed lines corespond to count rates smaller than 4 at least in one of the velocity directions along or perpendicular to the magnetic field.) It should be noted that the distribution function with the narrow strahl shown in Figure 2*a* has been constructed by superposition of data from eight cycles of measurement, distributed within an observation time of 23 min. The distribution function shown in Figure 1 has been derived from one of those eight cycles. Thus the distribution functions shown in Figure 1 and 2*a* pertain to the same observation time although with different time resolutions (20 s and 23 min, respectively), and comparison of the contour plot in Figure 1 with that of Figure 2*a* demonstrates the improvement of angular resolution.

3.1. *Pitch Angle Distributions*

The anisotropies of the distribution functions shown in Figure 2 can be seen more clearly in the corresponding pitch angle distributions. Figure 3*a* presents pitch angle distributions at different kinetic particle energies E for the distribution function with the narrow strahl shown in Figure 2*a*. Each plot in Figure 3*a* shows the phase space density $F(E, \alpha_p)$ in relative units as a function of pitch angle α_p for a constant particle energy E. The asterisks indicate the phase space density as determined from the individual channels of measurement, and the solid lines are proper fits to the data. The pitch angle of 0° corresponds to a particle motion directed along the magnetic field away from the sun. The count rates Z_{Max} corresponding to the maximum phase space density F_{Max} for each pitch angle distribution are much larger than 1, being of the order of 10^3 to 10^4 for all energies E, except for the largest energy $E = 847.5$ eV where we still have $Z_{\mathrm{Max}} = 77$. Thus the statistical uncertainty for the maximum phase space density F_{Max} in each plot given by the factor $1 \pm 1/(Z_{\mathrm{Max}})^{1/2}$ is quite small. Since for each constant energy E the count rate Z is porportional to the phase space density F according to $Z \sim FE^2$, the statistical uncertainty is small also for the phase space density at other pitch angles at least insofar as the relative phase space density F/F_{Max} is larger than say 10^{-2} for $E < 847.5$ eV and larger than 10^{-1} for $E = 847.5$ eV.

Figure 3*a* shows that for energies up to about 50 eV the pitch angle distributions are roughly symmetric (within a factor of 2 for the phase space density) with respect to particle velocities directed along the magnetic field away from the sun and toward the sun, although they are not isotropic. However, for larger energies they are extremely asymmetric. Here most of the electrons move away from the sun with small pitch angles. This is why this feature has been named the "strahl" (beam). This conclusion would also hold if we had plotted the pitch angle distributions in the solar wind rest frame rather than in the peak rest frame (see also Table 1).

We define an equivalent angular width W of the distribution by integrating $F/F_0 \sin \alpha_p \cos \alpha_p$ with $F_0 = F(E, \alpha_p = 0°)$ from the pitch angle $\alpha_p = 0$ to $\alpha_p = 90°$, i.e.,

$$W = \arcsin \left\{ \left[2 \int_0^{\pi/2} F/F_0 \sin \hat{\alpha}_p \cos \hat{\alpha}_p \, d\hat{\alpha}_p \right]^{1/2} \right\} \text{ degrees} \tag{1}$$

Here $\hat{\alpha}_p$ is the pitch angle in radian measure, and W is taken in units of degrees.

In case of a pitch angle distribution with $F = F_0 = \text{const}$ for $0 \le \alpha_p \le W_0$ and $F \equiv 0$ for $\alpha_p > W_0$ the equivalent width as defined by equation (1) is just given by $W = W_0$. In Table 1 we have given W for the different pitch angle distributions shown in Figure 3*a* and for additional pitch angle distributions (at energies of about 300 eV and 600 eV) pertaining to the same distribution function shown in Figure 2*a*.

In fact, W may be statistically uncertain to some extent if the count rates in an individual channel of measurement as calculated from the phase space density $F(E, \alpha_p)$ are of the order of 1 or lower for some pitch angles $\alpha_p \le 90°$. In order to indicate the range of this uncertainty we have calculated for each pitch angle distribution two values of W according to equation (1): one value W with F/F_0 as shown in the plots of Figure 3*a* and a second one $\hat{W}$ where we have set $F \equiv 0$ if the corresponding count rates are equal to 1 or smaller. If both angular widths deviate by more than 1° from each other, we indicate in Table 1 also the second value $\hat{W}$ within parentheses.

Feldman et al. [1978, 1982] have found similar pitch angle distributions from IMP data for high-speed streams near the orbit of earth. In the energy range from 62 eV to 247 eV they found from Gaussian fits to the pitch angle distributions an FWHM angular width for the strahl decreasing with increasing energy down to 15.5° or 12°. They argue that these pitch angle distributions are consistent with the predictions of exospheric theory for the more energetic electrons where the electrons may become collisionless above an exospheric base at about 10 to 30 solar radii away from the sun. Of course, Coulomb collisions are unavoidably present. However, since the mean free path for these energetic electrons due to Coulomb collisions is large compared to the distance from the sun, they should have only a minor effect. From theoretical calculations a narrow strahl results also if Coulomb collisions are taken into account [*Olbert*, 1983]. The pitch angle distribution shown in Figure 3*a* and in Table 1 indicate that the angular width of the strahl may even decrease to less than 5° for energies well above 500 eV. Such a small angular width is already below the estimated upper limit of roughly 10° to 15° for the angular resolution, and thus the actual angular width may be even smaller.

In Table 1 we give for each pitch angle distribution also the ratios $F(E, \alpha_p = 0°)/F(E, \alpha_p = 180°)$ and $F(E, \alpha_p = 180°)/F(E, \alpha_p = 90°)$ as derived with respect to the peak rest frame and to the solar wind rest frame. The ratios $F(E, \alpha_p = 0°)/F(E, \alpha_p = 180°)$ show that for a particle energy above about 100 eV there are of the order of 100 to 1000 more electrons moving along the magnetic field away from the sun than toward the sun. Such a result is expected if the electrons can escape from the sun along open magnetic field lines without strong scattering. However, it can also be seen from Table 1 that there is a tendency for the phase space density $F(E, \alpha_p = 180°)$ of backstreaming electrons to be about a factor of 2 to 4 larger than the phase space density $F(E, \alpha_p = 90°)$ of electrons moving perpendicular to the magnetic field at all energies. Such an anisotropy can hardly be explained by mere scattering of electrons toward the sun nor by reflection of electrons by the interplanetary electrostatic potential, which should trap only electrons with energies below 50 to 100 eV (see discussion below). Instead this is what we would expect if the magnetic field lines would form loops which extend from the sun outward to distances beyond the position of the spacecraft so that electrons can be guided back along closed magnetic field structures.

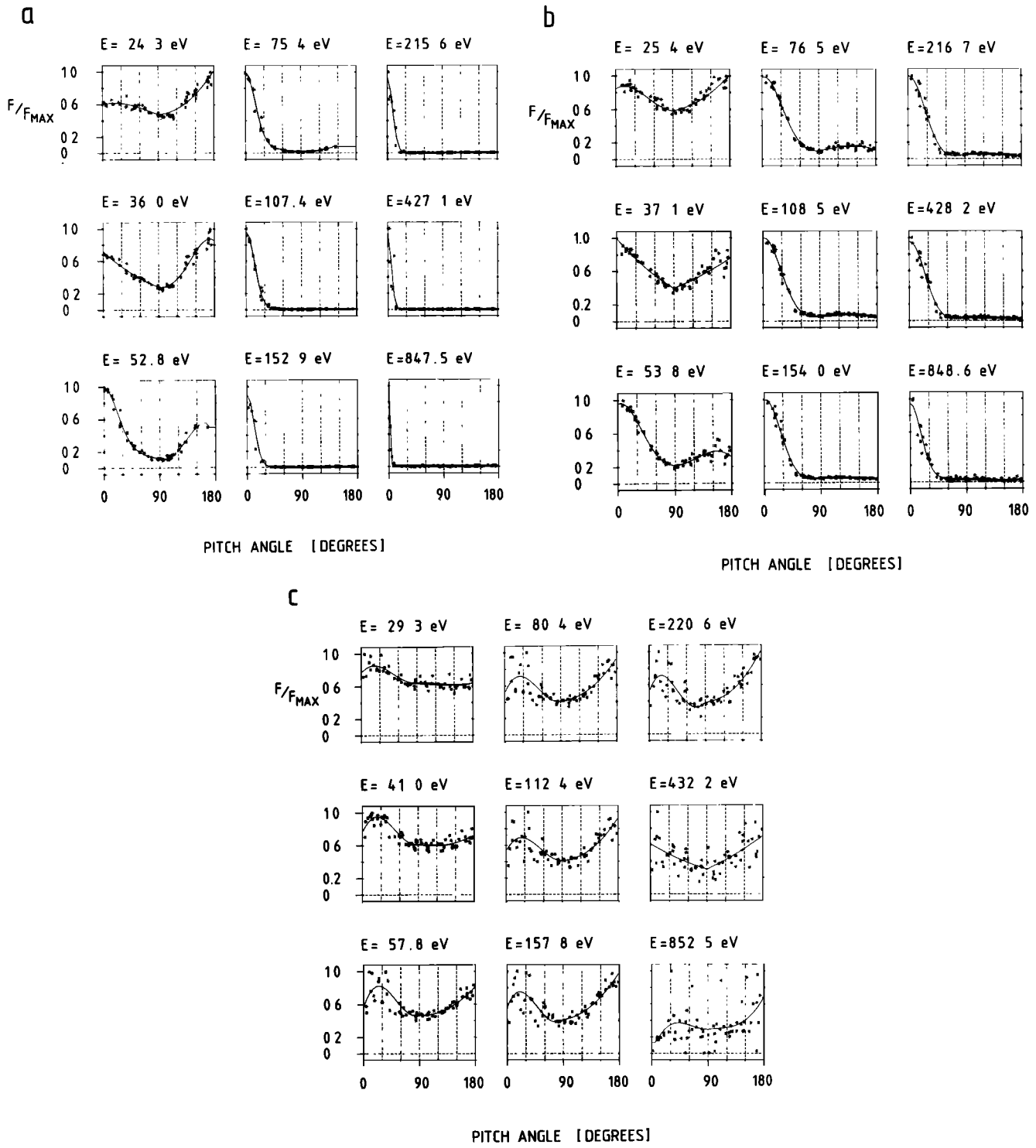

Fig. 3. Pitch angle distributions at different kinetic electron energies E for the three distribution functions presented by contour plots in Figure 2: (*a*) Distribution function with the narrow strahl (presented in Figure 2*a*). (*b*) Distribution function with the broad strahl (presented in Figure 2*b*). (*c*) Nearly isotropic distribution function (presented in Figure 2*c*). The pitch angle of zero degrees corresponds to a particle motion directed along the magnetic field away from the sun. Each pitch angle distribution shows the phase space density $F(E, \alpha_p)$ in relative units as a function of pitch angle α_p for constant particle energy E as observed in a frame of reference moving with the maximum of each distribution function, respectively. The velocities $\mathbf{V}_{e,\mathrm{Max}}$ of the maxima of the anisotropic electron distribution functions are somewhat shifted relative to the solar wind bulk velocity. Taking the proton bulk velocity $\mathbf{V}_p$ to be the center of mass velocity (i.e., neglecting alpha particles and heavier ions and assuming zero current condition), this shift is approximately $|\mathbf{V}_{e,\mathrm{Max}} - \mathbf{V}_p|$. Assuming $\mathbf{V}_p$ to be directed in the radial direction, we find approximately $|\mathbf{V}_{e,\mathrm{Max}} - \mathbf{V}_p| \approx$ 39 km s^{-1} for Figure 3*a* and $|\mathbf{V}_{e,\mathrm{Max}} - \mathbf{V}_p| \approx 265$ km s^{-1} for Figure 3*b*; $|\mathbf{V}_{e,\mathrm{Max}} - \mathbf{V}_p| \approx 3$ km s^{-1} for Figure 3*c* is not significantly different from zero.

TABLE 1. Parameters of Pitch Angle Distributions for the Distribution Function Shown in Figure 2*a*

Energy, eV	Angular Width $W(\hat{W})$, deg	$F(E, \alpha_p = 0°)/F(E, \alpha_p = 180°)$ Peak	SW	$F(E, \alpha_p = 180°)/F(E, \alpha_p = 90°)$ Peak	SW
24.3	80	0.6	0.5	2.1	2.4
36.0	53	0.8	0.7	3.0	3.5
52.8	37	2.0	1.5	4.6	5.7
75.4	25	13.0	8.9	6.2	7.8
107.4	19	122.7	81.8	4.2	5.7
152.9	16	268.7	217.7	2.7	3.2
215.6	12	464.1	379.9	3.5	4.0
304.3	11	675.4	542.0	2.7	3.1
427.1	8	672.7	593.3	2.3*	2.6*
599.7	2	803.1*	672.9*	3.0*	3.2*
847.5	6 (2)	67.2*	50.2*	1.5*	1.6*

The "peak" and "SW" labels in the last four columns refer to evaluations relative to the rest frame of the peak of the electron distribution function and the solar wind rest frame, respectively.

*Not statistically reliable since here the count rates in one channel of measurement near the pitch angles $\alpha_p = 180°$ and/or $\alpha_p = 90°$, respectively, are smaller than 2.

There are other possible processes which could lead to such an anisotropy for backstreaming electrons. For example, focusing of backscattered electrons by moving from a region of higher magnetic field strength at some place topologically beyond the point of observation into a region of lower magnetic field strength at the point of observation could cause such an anisotropy [*Ogilvie and Scudder*, 1981].

It is interesting to compare the pitch angle distributions in Figure 3*a* with the corresponding pitch angle distributions for the moderately anisotropic as well as the isotropic distribution functions. Figure 3*b* shows analogous pitch angle distributions for the distribution function presented in Figure 2*b*. The count rates are mostly large compared to 1 (Z_{Max} being well above 200 for most particle energies and being still 31 for the largest energy $E = 848.6$ eV), so that the pitch angle distributions are largely statistically significant except for the pitch angles outside the peak for the energy $E = 848.6$ eV where the count rates become of the order of 1.

Again the pitch angle distributions are roughly symmetric at low energies ($E \leq 40$ eV) and are strongly asymmetric for energies above 100 eV. However, in contrast to Figure 3*a* the angular widths of the peaks at small pitch angles are rather broad for all energies and become only slightly smaller with increasing energy (see Table 2 for the equivalent angular widths). (Similar pitch angle distributions with a broad peak in the energy regime of the halo for the slow solar wind have also been found by *Feldman et al.* [1978].) In addition there is a relatively high and nearly isotropic background of electrons at larger pitch angles where the ratios $F(E, \alpha_p = 0°)/F(E, \alpha_p = 180°)$ are smaller, being typically 10 to 100 for $E \geq 100$ eV, and $F(E, \alpha_p = 180°)/F(E, \alpha_p = 90°)$ is no longer significantly larger than 1 (see Table 2). The broadening of the strahl should be due to increased scattering processes experienced by the electrons on their way from the sun to the spacecraft.

Finally, Figure 3*c* shows the pitch angle distributions for the nearly isotropic distribution function presented in Figure 2*c*. Also these pitch angle distributions are statistically significant except for the one at the highest energy $E = 852.5$ eV where the count rates are of the order of 1. These more or less isotropic distributions indicate that scattering processes should have been quite effective here. The slight bidirectional anisotropy observed at nearly all energies above 50 eV might be an indication that the electrons have been observed on magnetic field loops, although different explanations are also possible [e.g., *Ogilvie and Scudder*, 1981]. If so, these loops either could be disconnected from the sun or could be connected to the sun but extending with their outer ends near the spacecraft. (For a review of observations indicating closed magnetic field structures in the solar wind, see *Pilipp* [1983].)

3.2. *Variation of Phase Space Density With Particle Energy*

According to earlier investigations each solar wind electron distribution may be divided into two components: a cool component (core) at low particle energies being represented fairly well by its Maxwellian fit and a hot component (halo) at larger particle energies being significantly elevated above this Maxwellian fit to the cool component and showing a flatter decrease for increasing particle energy [*Montgomery et al.*, 1968]. The core has been fitted by the product of a bi-Maxwellian and a truncated series expansion in odd powers of the thermal velocity, and the halo by a bi-Maxwellian [*Feldman et al.*, 1974, 1975, 1978], or both components by Maxwellians [*Ogilvie and Scudder*, 1978].

Two components may be discerned also for the distribution functions observed by Helios. Figure 4*a* shows a one-dimensional cut through the distribution function with the narrow strahl (Figure 2*a*) along a straight line in velocity space. This line goes through the maximum of the distribution function and is parallel to the magnetic field **B** for the left-hand plot and perpendicular to the magnetic field **B** for the right-hand plot. In other words, the left-hand plot of Figure 4*a* shows the phase space density $F(E = m(V_\parallel{}^2 + V_\perp{}^2)/2, \alpha_p = \arctan(V_\perp/V_\parallel))$ as a function of $V_\parallel$ at $V_\perp = 0$, and the right-hand plot shows F as a function of $V_\perp$ at $V_\parallel = 0$, where $V_\parallel$ and $V_\perp$ are the velocity components parallel and perpendicular to the magnetic field, respectively, and m is the electron mass. The dashed parabolas represent bi-

TABLE 2. Parameters of Pitch Angle Distributions for the Distribution Function Shown in Figure 2*b*

Energy, eV	Angular Width W, deg	$F(E, \alpha_p = 0°)/F(E, \alpha_p = 180°)$ Peak	SW	$F(E, \alpha_p = 180°)/F(E, \alpha_p = 90°)$ Peak	SW
25.4	71	0.8	0.6	1.7	2.3
37.1	54	1.3	0.6	1.9	2.9
53.8	50	3.1	1.1	1.4	3.1
76.5	42	9.8	3.8	1.0	2.1
108.5	37	27.8	13.3	0.6	1.1
154.0	35	28.3	16.4	0.6	0.9
216.7	34	40.6	20.3	0.5	0.8
305.4	33	35.4	21.9	0.6	0.8
428.2	32	56.0	31.5	0.4	0.6
600.8	29	100.1*	65.8*	0.3*	0.4*
848.6	26	23.6*	17.9*	1.4*	1.3*

The "peak" and "SW" labels in the last four columns refer to evaluations relative to the rest frame of the peak of the electron distribution function and the solar wind rest frame, respectively.

*Not statistically reliable since here the count rates in one channel of measurement near the pitch angles $\alpha_p = 180°$ and/or $\alpha_p = 90°$, respectively, are smaller than 2.

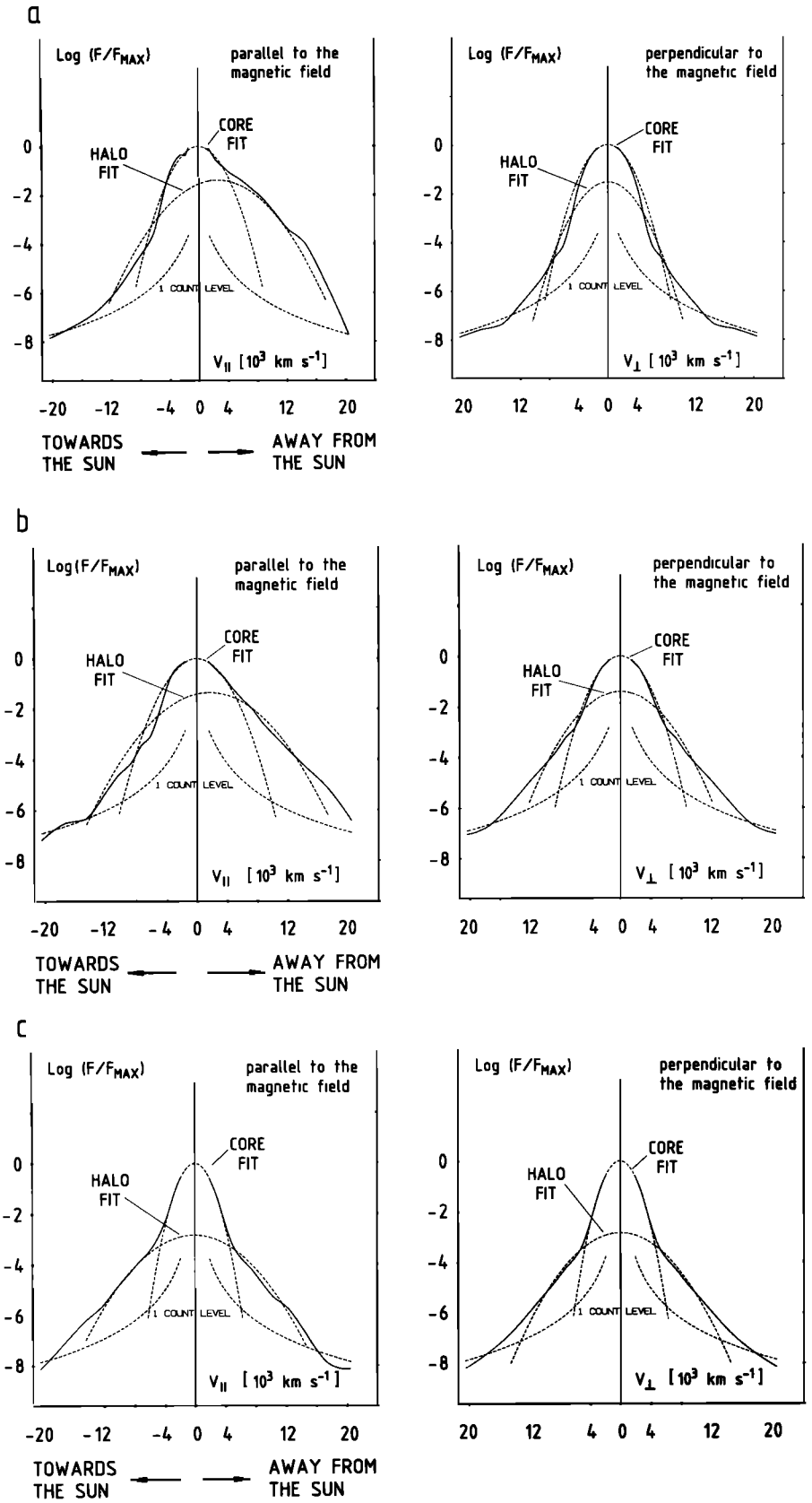

Fig. 4. One-dimensional cuts through the three distribution functions presented in Figure 2 are shown. Each plot shows the phase space density along a straight line in velocity space, which is parallel or perpendicular to the magnetic field and goes through the maximum of the respective distribution function. Core and halo fits as well as the one-count levels are indicated by dashed lines. (*a*) Distribution function with the narrow strahl. (*b*) Distribution function with the broad strahl. (*c*) Nearly isotropic distribution function.

Maxwellian fits to the low energy part of the distribution function (core fit) and to the high energy part (halo fit). In particular, the core fit with temperatures $T_{c\parallel} = 1.9 \times 10^5$ K and $T_{c\perp} = 1.7 \times 10^5$ K parallel and perpendicular to the magnetic field, respectively, pertains to the distribution function as observed in the second and third energy channels with energies of about 10 eV and 16 eV (after having corrected for the spacecraft potential, which for this particular example is about 5 V), corresponding to velocities of 1.9×10^3 km s^{-1} and 2.4×10^3 km s^{-1}. The halo fit with the parallel temperature $T_{h\parallel} = 6.3 \times 10^5$ K and the perpendicular temperature $T_{h\perp} = 2.7 \times 10^5$ K is a fit to the distribution function at energies above 107 eV or above a velocity of 6.1×10^3 km s^{-1}. As has been discussed in section 2, core fits have been used to supplement the distribution functions at energies below 10 eV if reliable measurements are not available. Finally, the phase space density corresponding to the one-count level is also indicated by dashed lines. The observed distribution functions are statistically reliable only well above this one-count level.

For the distribution function shown here, a cool core at low particle energies can be distinguished reasonably well from a hotter halo at larger particle energies in agreement with earlier investigations. However, a significant break in the slope of the distribution function separating the core from the halo may be discerned only for velocity directions different from the strahl direction. For the velocity directions along the magnetic field toward the sun and perpendicular to it the breakpoint energy E_B characterizing the sudden change of the slope may be roughly 100 eV, corresponding to a breakpoint velocity V_B of about 6×10^3 km s^{-1}. If we define the breakpoint energy as the intersection between the core fit and the halo fit, which is also about the energy above which the measured phase space density is significantly elevated above the core fit, then we find for these velocity directions the somewhat higher breakpoint energies E_B = 124 eV and 135 eV, respectively.

Similar conclusions can be drawn for the moderately anisotropic distribution function with the broad strahl (Figure 2*b*) whose phase space density has been plotted versus particle velocity along **B** and perpendicular to it in Figure 4*b*. Finally, Figure 4*c* shows the variation of the phase space density with particle velocity for the isotropic distribution function (Figure 2*c*). Here the distinction between core and halo can clearly be made for all velocity directions, and a breakpoint energy E_B at about 60 eV corresponding to a velocity of 4.6×10^3 km s^{-1} is clearly discernible. In addition the core is fitted rather well by a Maxwellian where the parallel and perpendicular temperatures $T_{c\parallel} = 0.916 \times 10^5$ K and $T_{c\perp} = 0.910 \times 10^5$ K of the bi-Maxwellian core fit are almost identical.

Thus according to Helios observations the electron distribution functions may roughly be decomposed into a cool component and a hot component although a breakpoint energy with respect to the change of the slope cannot be discerned along the strahl direction for anisotropic distribution functions. Note, however, that description of each electron distribution function by a superposition of the core fit and of the halo fit represents only a simplified model distribution. Deviations of the observed distribution functions from these model distributions may provide more information about the propagation conditions for the electrons. In particular, microinstabilities in the solar wind may depend decisively on the fine details of the distribution functions [*Dum et al.*, 1980].

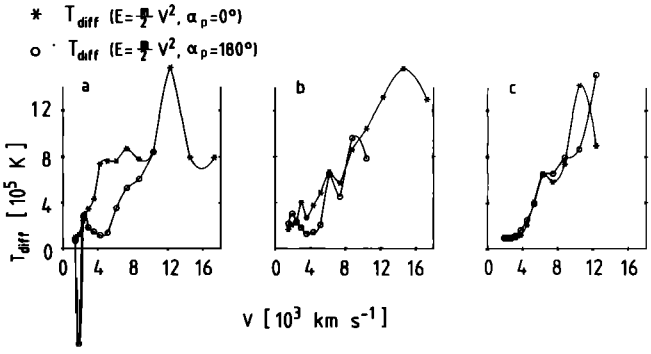

Fig. 5. Differential temperatures as defined in the text are plotted as functions of electron velocity for $\alpha_p = 0°$ and $\alpha_p = 180°$ for the three distribution functions shown in Figures 2*a*–2*c*. Again E and α_p are defined in the peak rest frame of the respective distribution function. (*a*) Distribution function with the narrow strahl. (*b*) Distribution function with the broad strahl. (*c*) Nearly isotropic distribution function.

A sensitive indicator for deviations of a considered distribution function from a Maxwellian or from a superposition of two Maxwellians may be the differential temperature T_{diff}, defined by

$$T_{diff}(E, \alpha_p) = -\left(\kappa \frac{d \ln F(E, \alpha_p)}{d E}\right)^{-1}$$

with κ being Boltzmann's constant. By definition, T_{diff} is constant for a Maxwellian and is equal to the temperature. If the distribution function is a superposition of two Maxwellians, a Maxwellian with the lower temperature T_c dominating the distribution function at low particle energies and a Maxwellian with the higher temperature T_h dominating the distribution function at larger energies, then this differential temperature T_{diff} should be roughly constant with $T_{diff} \approx T_c$ at low energies but increase to T_h at larger energies, again being nearly constant at large energies. In contrast, if T_{diff} is strongly varying with energy E at all energies (in the frame of reference where the maximum of the distribution function is at rest), the considered distribution function can hardly be represented by Maxwellians in detail.

In Figure 5 we have plotted $T_{diff}(E, \alpha_p = 0°)$ by asterisks and $T_{diff}(E, \alpha_p = 180°)$ by circles as a function of particle velocity $V = (2E/m)^{1/2}$. Only measured points have been accepted for this plot where the count rates are clearly above the one-count level. Figures 5*a*, 5*b*, and 5*c* show T_{diff} for the measured distribution functions presented in Figures 4*a*, 4*b*, and 4*c*. The differential temperatures $T_{diff}(E, \alpha_p = 0°)$ and $T_{diff}(E, \alpha_p = 180°)$ derived from model distributions constructed by superpositions of the respective core and halo fits are presented in Figures 6*a*, 6*b*, and 6*c*, where also the temperature $T_{c\parallel}$ parallel to the magnetic field of the respective core fit and the parallel temperature $T_{h\parallel}$ of the respective halo fit are indicated by the dashed lines. For the superposed model distributions the differential temperatures at particle energies well below the breakpoint energy E_B are nearly equal to the core fit temperatures $T_{c\parallel}$. In contrast, for energies sufficiently above E_B the differential temperatures are mainly determined by the halo fit. Note that the halo fit is shifted along the magnetic field away from the sun relative

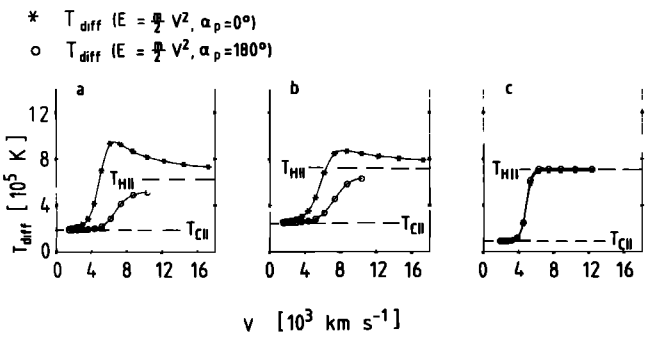

Fig. 6. Differential temperatures as defined in the text as functions of electron velocity for $\alpha_p = 0°$ and $\alpha_p = 180°$ for the superpositions of core fit and halo fit of the three distribution functions shown in Figures 2*a*–2*c*, respectively. The temperatures parallel to the magnetic field of the respective bi-Maxwellian core fits and halo fits are indicated by horizontal dashed lines. (*a*) Distribution function with the narrow strahl. (*b*) Distribution function with the broad strahl. (*c*) Nearly isotropic distribution function.

to the core fit by 2584 km s^{-1} in Figure 4*a*, by 1655 km s^{-1} in Figure 4*b*, and by 107 km s^{-1} in Figure 4*c*. This means that the contribution of the halo fit to T_{diff} becomes larger than $T_{h\parallel}$ in the direction away from the sun and smaller than $T_{h\parallel}$ in the direction toward the sun.

Comparison of Figure 5 with Figure 6 shows that the differential temperature for the observed distribution functions behaves much more irregularly than the differential temperature for the fits. Clear-cut core and halo temperatures as indicated in Figure 6 are mostly not detectable in Figure 5. The anisotropic distribution functions (Figures 5*a* and 5*b*) do not show a definite core temperature. T_{diff} increases more or less continuously with the velocity in the strahl direction at least for low velocities, and it fluctuates quite strongly in the opposite direction, showing a minimum near the breakpoint velocity. There is an indication for a relatively constant halo temperature in Figure 5*a* (except for the strong peak near $V = 12 \times 10^3$ km s^{-1}) but not in Figure 5*b*. The isotropic distribution function shows a relatively well defined core temperature, but T_{diff} increases nearly monotonically at larger velocities.

We admit that not all details for T_{diff} are representative, since they could be produced by time variations of phase space density and of magnetic field direction during the cycles of measurement. In particular, the peak for T_{diff} near $V_\parallel = 12 \times 10^3$ km s^{-1} (or near the particle energy of about 410 eV) in Figure 5*a* could be due to a fluctuation of the direction of the actual magnetic field within the uncertainty of 5° to 10° relative to the time-averaged magnetic field direction (averaged over 16 s) that has been used within an individual cycle of measurement. Since the strahl is very narrow at particle energies of several hundred eV (see Figure 3*a*) with an angular width of the order of 10° or less, such fluctuations may lead to appreciable fluctuations of the observed phase space density along the direction of the average magnetic field and thus to fluctuations of T_{diff}. However, the following features, which do not fit a superposition of two bi-Maxwellians, seem to be significant: the steep increase of T_{diff} with energy in the strahl direction, at least in the energy regime of the core, and the minimum of T_{diff} in the opposite direction near the breakpoint energy for anisotropic distribution functions; in addition the steep increase of T_{diff} in the energy regime of the halo for isotropic and moderately anisotropic distribution functions. These deviations from the bi-Maxwellian model distributions may be important for more refined theories of electron propagation.

3.3. *The Electron Heat Flux*

As one should expect, the strahl in the distribution functions is associated with a large heat flux. In fact, the heat flux Q_e as derived from numerical integration is for the anisotropic distribution functions $Q_e = 11.5 \times 10^{-2}$ erg cm^{-2} s^{-1} (Figure 2*a*) and $Q_e = 4.0 \times 10^{-2}$ erg cm^{-2} s^{-1} (Figure 2*b*), respectively, whereas for the isotropic distribution function (Figure 2*c*) we find only $Q_e = 0.1 \times 10^{-2}$ erg cm^{-2} s^{-1}. The normalized heat flux values $Q_c = Q_e/\{N_e m(\kappa(T_{c\parallel} + 2T_{c\perp})/3m)^{3/2}\}$, being a measure for the skewing of the distribution functions, are $Q_c = 0.515$, 0.716, and 0.03, respectively (with N_e the electron number density). The contribution to the heat flux from electrons with different energies E can be seen from the partial heat flux

$$\hat{Q}(V) = 2\pi \int_0^V \int_{-1}^{+1} F(E' = m V'^2/2, \alpha_p') \cdot E' V' \cos \alpha_p' \, d \cos \alpha_p' V'^2 \, dV'$$

In Figures 7*a*, 7*b*, and 7*c* we have plotted the partial heat flux $\hat{Q}(V)$ for the distribution functions shown in Figures 2*a*, 2*b*, and 2*c*, respectively, up to velocities V for which the count rates in the strahl direction ($\alpha_p = 0°$) have been larger than 10. In Figures 7*a* and 7*b* the heat flux $\hat{Q}(V)$ is rather small in the core regime (i.e., for $V \lesssim 5 \times 10^3$ km s^{-1}) and increases strongly with energy in the strahl regime. The partial heat flux $\hat{Q}(V)$ for the isotropic distribution function shown in Figure 7*c* behaves differently, where $\hat{Q}(V)$ increases steeply in the energy regime of the core (i.e., $V < 5 \times 10^3$ km s^{-1}), but decreases at large energies in the halo regime (i.e., for $V > 8 \times 10^3$ km s^{-1}), so that the energetic electrons contribute a negative heat flux. Here the heat flux is probably not significantly different from zero. It seems that for the anisotropic distribution functions the partial heat flux approaches an asymptotic value for large velocities where the count rates are still reasonably high so that the instrument has probably observed nearly the entire heat flux. However, as has been shown by *Ogilvie et al.* [1971], $\hat{Q}(V)$ may

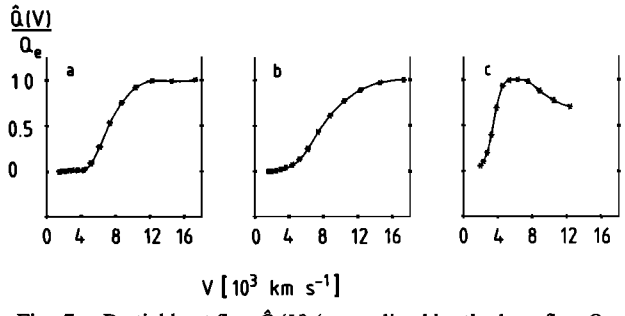

Fig. 7. Partial heat flux $\hat{Q}(V)$ (normalized by the heat flux Q_e as calculated from the entire distribution functions) as a function of $V = (2E/m)^{1/2}$. Here E and α_p are defined in the rest frame of the electron bulk motion (i.e., the solar wind rest frame if the motion of alpha particles and ions with larger masses relative to protons is neglected). (*a*) Distribution function with the narrow strahl. (*b*) Distribution function with the broad strahl. (*c*) Nearly isotropic distribution function.

increase up to energies of several keV far above the highest energy channel of the Helios instrument, so that the entire heat flux may sometimes be larger than observed here.

4. COMPARISON WITH THEORETICAL RESULTS

Historically, exospheric theory was the first theoretical approach in solar wind research which derived a strahllike feature and which introduced a distinction between two components in the electron distribution functions [*Jockers*, 1970; *Lemaire and Scherer*, 1971; *Schulz and Eviatar*, 1972; *Perkins*, 1973]. According to this theory each distribution function is composed of a component of trapped electrons, whose kinetic energy is below the escape energy with respect to the interplanetary electrostatic potential and which are therefore reflected back toward the sun, and of a component of free electrons, whose energy is above the escape energy and which propagate away from the sun to infinity. Starting with a Maxwellian distribution function for the electrons at an exospheric base near the sun, above which the electrons are assumed to propagate collisionlessly, the distribution function above this exospheric base is predicted to be a truncated Maxwellian. In the energy regime of the trapped electrons the predicted distribution function is symmetric about the origin of the frame of reference corotating with the sun; i.e., in the corotating frame there are as many electrons moving away from the sun as electrons moving toward the sun. In particular, the peak of the distribution function is predicted to be at rest, implying that the peak is shifted relative to the solar wind bulk velocity along the magnetic field toward the sun by $U_{SW} = (V_{SW}^2 + \Omega^2 R^2)^{1/2}$ where V_{SW} is the solar wind velocity in the inertial rest frame of the sun, Ω is the angular velocity of the sun, and R is the distance from the sun [see also *Hollweg*, 1974, 1976]. The trapped electrons which are emitted from the exospheric base return to it after reflection by the electrostatic potential, forming an anisotropic but symmetric distribution function. However, an isotropic distribution function in the energy regime of the trapped electrons is also consistent with exospheric theory if a proper number of electrons trapped between the electrostatic potential barrier and the magnetic mirror of the interplanetary magnetic field above the exospheric base are added. In contrast, the distribution function in the energy regime above the escape energy is predicted to be extremely asymmetric and anisotropic and to be different from zero only in a narrow region of velocity space along the magnetic field in the antisolar direction. Namely, all free electrons should move away from the sun with decreasing pitch angles.

It seems suggestive to identify trapped electrons with the roughly symmetric core of the observed distribution functions and the free electrons with the observed strongly asymmetric and anisotropic halo. Of course, Coulomb collisions are unavoidably present and should modify or even drastically change this simple picture, in particular at low energies. Also anomalous processes and a different magnetic field topology may lead to electron distribution functions different from those predicted by exospheric theory. Nevertheless, this theory provides insight into some mechanisms causing important structural details of the distribution functions, in particular the strahl.

The exospheric picture has been modified by various attempts to include scattering effects. The helioclassical approach takes into account some scattering of the core electrons due to Coulomb collisions and/or various microinstabilities. These scattering processes should lead to a heat flux of the core [*Perkins*, 1973] and reduce the shift between the peak of the distribution functions and the solar wind velocity [*Hollweg*, 1974, 1976; *Feldman et al.*, 1979*b*].

A different approach to calculating the electron distribution functions has been proposed by *Scudder and Olbert* [1979*a*, *b*] and will be referred to as S-O theory. In this theory, scattering of electrons by Coulomb collisions is taken into account using a probability formalism, and the distinction between core and halo comes mainly from the large difference of the mean free paths between low energy electrons and electrons at higher energies. According to the S-O theory the core is the collisionally quasi-trapped electron component, and the halo the electron component leaking through the local medium, having a larger than 95% probability of transiting the local Coulomb mean free path without being scattered. Here the local Coulomb mean free path is taken as the Coulomb mean free path of an electron whose kinetic energy is the average thermal energy of the core electrons (defined by the temperature T_c of the core fit). This theory predicts the breakpoint energy E_B to be equal to about $7\kappa T_c$ as seen from the solar wind rest frame.

Another probability formalism describing scattering by Coulomb collisions has been developed by *Lemons and Feldman* [1983], who applied their formalism to electrons in the energy regime of the halo and calculated a collisionally modified angular width of the strahl. Finally, *Olbert* [1983] has calculated the forward part of the electron distribution functions (i.e., the distribution functions for the outward propagating electrons with $V_\parallel > 0$), describing the propagation of the electrons by the Boltzmann equation and representing the collision term by Krook's approximation, considering Coulomb collisions as the only collision processes.

All these theories take into account the interaction of the electrons with the interplanetary electrostatic field. In fact, this electrostatic field is mainly a consequence of the electron pressure gradient as can be seen from the equation of motion for the electrons or from the generalized Ohm's law [e.g., *Scudder and Olbert*, 1979*a*, *b*] and thus should be explicitly taken into account in any theory treating the electrons as an individual component of solar wind plasma. These theories are also based on the common assumption that the electrons move along open magnetic field lines, i.e., on field lines which extend from the sun to infinity. They differ from each other mainly by different assumptions and approximations with respect to scattering processes. The electron distribution functions, which have been theoretically derived so far, are all strongly anisotropic and asymmetric in the energy regime of the halo; i.e., they all show a strahl. Thus the observed strahl is qualitatively consistent with these theories, although a few electrons may have been guided back toward the sun by closed magnetic field lines as discussed in connection with Figure 3*a*. A nearly isotropic distribution function with a slight bidirectional anisotropy as shown in Figure 2*c* has not been derived by any of these theories. Here the slight bidirectional anisotropy in the pitch angle distributions (Figure 3*c*) may indicate that the electrons are trapped in closed magnetic field structures as discussed above. The near isotropy indicates that scattering processes should be very effective at all particle energies.

We compare now several predicted details of the electron distribution functions with the observed results.

At first we consider the velocity shift of δV_c between the peaks of the distribution functions and the electron bulk velocity (where the electron bulk velocity is assumed to be identical with the solar wind bulk velocity). Here we find a clear discrepancy between the predictions of exospheric theory and observations. Although for the distribution functions with the strahl both the predicted shift and the observed shift are in the same direction, i.e., they are directed along the magnetic field toward the sun, this shift is observed to be much smaller than the solar wind bulk velocity U_{SW} in the corotating frame of reference. For the distribution function with the narrow strahl (Figure 2*a*) we find $\delta V_c = 102.3$ km s^{-1} being much smaller than $U_{SW} = 703$ km s^{-1}, and for the distribution function with the broad strahl (Figure 2*b*) we find $\delta V_c = 301$ km s^{-1} whereas $U_{SW} = 579$ km s^{-1}. For the nearly isotropic distribution function (Figure 2*c*) the shift $\delta V_c = 4.2$ km s^{-1} is probably not significantly different from zero. Similar discrepancies between the observed shift and the shift predicted by exospheric theory have been found by *Montgomery* [1972*b*] and *Feldman et al.* [1975].

However, we remind the reader that the small shift between the peak and the bulk velocity was not immediately measured but was inferred from the bi-Maxwellian core fit. For the distribution function with the narrow strahl the core fit shown in Figure 4*a* is a fit to the distribution function as measured in the two energy channels at $E \approx 10$ eV and $E \approx 16$ eV (after correction for the spacecraft potential of about 5 V), and thus the peak of this core fit describes the average velocity of the core electrons in the energy range between 10 and 16 eV. Since even the low energy part of this distribution function deviates from a Maxwellian, the bi-Maxwellian core fit might sensitively depend on the energy range where the measurements have been taken into account for this core fit. Therefore we have also calculated bi-Maxwellian core fits (not shown in Figure 4*a*) which have been fitted to the distribution function as observed in more energy channels, i.e., to the distribution function as observed in the three energy channels at $E = 10$, 16, and 24 eV, in the four energy channels at $E = 10$, 16, 24, and 36 eV, and finally in the five energy channels at $E = 10$, 16, 24, 36, and 53 eV. Fortunately, the core density N_c and the core temperatures $T_{c\parallel}$, $T_{c\perp}$ due to these four different core fits (including the one shown in Figure 4*a*) vary only slightly from $N_c = 58.5$ cm^{-3} to 53.7 cm^{-3}, from $T_{c\parallel} = 1.9 \times 10^5$ K to 2.1×10^5 K, and from $T_{c\perp} = 1.7 \times 10^5$ K to 1.4×10^5 K. However, the velocity shift δV_c varies more sensitively, increasing from $\delta V_c = 102$ km s^{-1} to 182 km s^{-1} and to 208 km s^{-1} and then decreasing to 140 km s^{-1} if the core fits are considered in succession of increasing number of energy channels taken into account. (If we include additional energy channels of still larger energy for the core fits, then the strahl influences these fits appreciably, and then $T_{c\parallel}$ is strongly increased and δV_c is further decreased, eventually becoming negative.) From these fits we see that the shift δV_c between the average velocity of the core electrons and the bulk velocity of all electrons is significantly smaller than $U_{SW} = 703$ km s^{-1}, at least for the energy range within the core regime where reliable measurements are available. Also for the distribution function with the broad strahl, four different core fits have been calculated with the energy range from $E = 11$ eV to 17 eV, from $E = 11$ eV to 25 eV, from $E = 11$ eV to 37 eV, and from $E = 11$ eV to 54 eV, respectively. Only the first one is shown in Figure 4*b*. Again the core densities and core temperatures vary only slightly for the different fits, but the shift δV_c varies from 301 km s^{-1} to 313 km s^{-1}, 266 km s^{-1}, and 180 km s^{-1}. Also here the shift δV_c is significantly smaller than $U_{SW} = 579$ km s^{-1} for all of these core fits.

It has been argued by *Feldman et al.* [1976*a*, *b*, 1979*b*] that the shift may be controlled by microinstabilities where at least during some observation times, δV_c is about the Alfvén speed V_A. In fact, for the distribution function in Figure 2*a* we have $V_A = 183.4$ km s^{-1}, which agrees reasonably well with the observed shift, and for the distribution function in Figure 2*b* we have only $V_A = 84.3$ km s^{-1}, which is much lower than the observed shift. Thus, at least for the anisotropic distribution functions, observations are consistent with the hypothesis that δV_c is controlled by some microinstabilities limiting the shift to the Alfvén velocity or to a larger value [see also *Schulz and Eviatar*, 1972; *Perkins*, 1973].

On the other hand the shift could also be controlled by Coulomb collisions only. *Feldman et al.* [1979*b*] have estimated the shift δV_c on the basis of the helioclassical picture and find that Coulomb collisions between core electrons and protons as well as wave-particle interactions could reduce this shift to the observed values. However, the helioclassical picture takes into account only the local scattering frequencies, whereas nonlocal scattering processes should be important [*Scudder and Olbert*, 1979*a*, *b*]. In addition, as discussed by Feldman et al., the results of this helioclassical theory depend sensitively on the bounce periods of the trapped electrons, which are very uncertain. Thus comparison of the shift as derived from helioclassical formulas with the observed shift does not allow a definite conclusion for the dominant interaction processes of the core electrons. All that we can conclude from our results is that at least for the distribution functions with a strahl the shift is drastically reduced by frictionlike interaction processes between core electrons and protons. In a future paper we will discuss these points in more detail.

A second feature of the observed distribution functions which may be compared with theory is the breakpoint energy E_B separating the core from the halo. According to exospheric theory the electron distribution function should vary smoothly along the strahl direction from low to high particle energies without any break between core and halo. In contrast, for velocity directions opposite to the strahl the distribution function should drop to zero above the escape energy with respect to the interplanetary electrostatic potential. Similarly, for velocity directions perpendicular to the strahl the distribution function is predicted to drop to zero above an energy smaller than or equal to the escape energy. Thus, a sudden drop or break should be seen in the distribution functions marking the upper energy limit for the core where the breakpoint energy is given by $e\phi$ with the electrostatic potential ϕ, at least for the velocity direction opposite to the strahl.

On the other hand, as has been discussed by *Scudder and Olbert* [1979*b*], a break between core and halo may be decisively determined by Coulomb collisions. Then a break in the slope of the distribution functions should occur for all velocity directions. Scudder and Olbert predict the break to occur at an energy of about $7\kappa T_c$ (with T_c being the core temperature).

In fact, as has been discussed above, there is a significant break in the slope for the nearly isotropic distribution

function shown in Figure 4*c* for all velocity directions. The breakpoint energy is about 60 eV, in reasonable agreement with the breakpoint energy of $7\kappa T_{c\parallel} \approx 7\kappa T_{c\perp} \approx 55$ eV predicted by the S-O theory. Here the distribution function is represented rather well by the nearly Maxwellian core fit at energies well below the breakpoint energy and is significantly elevated above this fit at larger energies.

On the other hand, the anisotropic distribution functions show a clear-cut break between core and halo only for velocity directions opposite to the strahl and perpendicular to it but not along the strahl direction (see Figures 4*a* and 4*b*). In addition, for velocity directions opposite to the strahl and perpendicular to it, the anisotropic distribution functions drop significantly below the core fit at energies somewhat below the breakpoint energy and are elevated above this fit only at energies well above the breakpoint energy. From Figures 5*a* and 5*b* it can be seen that the differential temperatures show significant minima at energies somewhat below the breakpoint energy for the velocity direction opposite to the strahl (at $\alpha_p = 180°$). This fact indicates a maximum decline with energy of the distribution functions there. These features of the anisotropic distribution functions are to some extent similar to characteristics predicted by exospheric theory. Collisions will tend to smear the predicted sudden drops. However, the relatively fast declines of the distribution functions as well as the minima of the differential temperature in solar direction may still be determined by the electrostatic potential. An upper limit for the escape energy as seen in the inertial rest frame of the sun has been estimated from the electron energy balance by neglecting magnetic forces in the solar wind [*Feldman et al.*, 1975]. Applying this estimate to the distribution function shown in Figure 2*a* or Figure 4*a*, we find an upper limit of 60 eV. This gives in a frame of reference moving with the peak of the distribution function an escape energy $E_T = 78$ eV (or the escape velocity $V_T = 5 \times 10^3$ km s^{-1}) for the direction opposite to the strahl. As can be seen from Figure 4*a*, the distribution function decreases significantly below the core fit in the energy range from about 70 eV up to an energy somewhat beyond the breakpoint energy (i.e., for velocities ranging from 5×10^3 km s^{-1} up to about 7×10^3 km s^{-1}) in the solar direction. Also the minimum of the differential temperature for the solar direction occurs at an energy of about 70 eV (or a velocity $V = 5 \times 10^3$ km s^{-1}) (see Figure 5*a*). Thus the relatively fast drop of the distribution function in the velocity direction opposite to the strahl occurs roughly at the estimated upper limit for the electrostatic potential. This agreement may be considered as satisfactory in view of the approximate procedure to determine E_T as well as the energy range for the fastest drop of the distribution function. Then we have observational support for the hypothesis that the boundary of the core is in fact determined to a large extent by the interplanetary electrostatic potential, i.e., by electrostatic reflection of the core electrons toward the sun. On the other hand, the halo electrons moving toward the sun with energies well above the escape energy should have been scattered back (with the possible exception of a few electrons which have been guided back by closed magnetic field structures as discussed above). Then the breakpoint energy, where the relatively sudden change of the slope for the distribution function occurs, should roughly mark the energy above which the phase space density of backscattered electrons dominates the phase space density of electrostatically reflected electrons. In this sense both the electrostatic potential and the scattering processes could determine the breakpoint energy.

Similar results can be found for the distribution function shown in Figure 4*b*. Here we find the escape energy $E_T \approx 87$ eV for the direction opposite to the strahl in the frame of reference moving with the peak of the distribution function. Figure 4*b* shows that the distribution function drops below the core fit at energies ranging from about 40 eV up to an energy somewhat beyond the breakpoint energy (i.e., for velocities ranging from about 3.8×10^3 km s^{-1} up to about 8×10^3 km s^{-1}). The minimum for the differential temperature in solar direction occurs at about 46 eV (or at the velocity 4×10^3 km s^{-1}). Thus we have again rough agreement between the escape energy and the energy for the relatively sudden drop of the distribution function in the velocity direction opposite to the strahl. Also here the breakpoint energy could roughly mark the energy above which the phase space density of the backscattered halo electrons dominates the phase space density of electrostatically reflected electrons. These results are consistent with observations from IMP data [*Feldman et al.*, 1975] where a breakpoint energy has been found which is somewhat larger than the escape energy (typically by 30 to 40%).

According to the S-O theory the breakpoint energy should be about $7\kappa T_c$ as seen in the solar wind rest frame. In fact, for the distribution function shown in Figures 2*a* and 4*a* we have $7\kappa T_{c\parallel} = 112$ eV, which gives a predicted breakpoint energy of 88.3 eV in the peak rest frame for the velocity direction opposite to the strahl. This may still be in rough agreement with the breakpoint energy of $E_B = 124$ eV as defined by the intersection between the core and halo fit or even better with the breakpoint energy of about $E_B = 110$ eV as judged by the eye from the break in the slope of the distribution function. For the distribution function shown in Figures 2*b* and 4*b* we have $7\kappa T_{c\parallel} = 148$ eV, which gives a predicted breakpoint energy of about 125 eV in the peak rest frame for the direction opposite to the strahl. Again this is in reasonable agreement with the breakpoint energy of $E_B = 149$ eV as defined by the intersection between the core fit and the halo fit or with the breakpoint energy of again $E_B \approx 110$ eV as judged by the eye.

However, as has been discussed by *Scudder and Olbert* [1979*b*], the predicted breakpoint energy of $7\kappa T_c$ should be approximately the escape energy with respect to the interplanetary electrostatic potential, if the electron temperatures may be approximated by the core temperature T_c and if this core temperature T_c decreases with distance R from the sun as $R^{-1/3}$ [see also *Ogilvie and Scudder*, 1978]. Although the solar wind is strongly variable in space and time and the radial variations of T_c may strongly vary (as will be shown from Helios data in a future paper), these estimates indicate that the escape energy E_T as well as the predicted breakpoint energy $7\kappa T_c$ should be of the same order of magnitude. Then we expect agreement at least within an order of magnitude between the breakpoint energy and $7\kappa T_c$ even if the break is determined to a large extent by the electrostatic potential.

Thus, although the experimental results provide some indications for possible mechanisms determining the breaks in the electron spectra, the detailed mechanisms as well as their relative importance are still unknown and may be different for different distribution functions. Trapping in the electrostatic potential, and in a few cases in closed magnetic

field structures, together with Coulomb collisions or even anomalous scattering processes may play an important role.

Finally, the angular width of the strahl as well as the ratios of phase space densities $F(E, \alpha_p = 0°)$ and $F(E, \alpha_p = 180°)$ in the energy regime of the strahl has been predicted by theories and can be compared with observations. Of course, $F(E, \alpha_p = 180°) = 0$, predicted by exospheric theory for the energy regime of the halo, is not observed since some scattering occurs even for the strahl electrons. However, the observed ratios $F(E, \alpha_p = 0°)/F(E, \alpha_p = 180°)$ can be extremely large for the distribution functions with a strahl, being of the order of 100 to 1000 for the distribution function with the narrow strahl and 10 to 100 for the distribution function with the broad strahl (see Tables 1 and 2). These results are in agreement with earlier findings by *Pilipp et al.* [1981] and with measurements from the IMP spacecraft [*Feldman et al.*, 1982]. Agreement with predictions of the S-O theory can be achieved only if inelastic collisions are important.

Lemons and Feldman [1983] have calculated the angular width of the strahl including the effect of elastic Coulomb collisions. Comparing their results with IMP observations, they found indications for anomalous scattering of strahl electrons even in the case of a narrow strahl. Indications for anomalous scattering processes come also from Helios observations. The distribution function with the broad strahl (Figure 2*b*) and the nearly isotropic distribution function (Figure 2*c*) provide evidence for anomalous scattering of electrons. On the other hand, following the procedure developed by Lemons and Feldman, we find only marginal indications for anomalous scattering in case of the distribution function with the narrow strahl (Figure 2*a*). In a future paper we present independent indications that anomalous scattering of strahl electrons should in fact occur even for distribution functions with a narrow strahl.

Finally, we mention that the electron distribution functions as calculated by *Olbert* [1983] are rather similar to the observed distribution functions with a narrow strahl. In particular, the angular width of the theoretically derived strahl decreases with particle energy in qualitative accordance with observations, reflecting the fact that scattering by Coulomb collisions becomes less and less effective for increasing particle energy. It may be interesting to note that these theoretically derived distribution functions show a second peak along the strahl direction in the transthermal energy range, which cannot be seen in the observed distribution functions (see Figure 4*a*). It is not clear whether this second peak is a special property of this one realization of the distribution function as calculated by Olbert or whether this feature is a more general property of distribution functions shaped by Coulomb collisions. If it is a general feature, then this discrepancy could be an indication for anomalous processes. As has been mentioned by Olbert, such a double peak should provide free energy for various plasma waves.

5. SUMMARY

We have discussed details of the shapes of electron distribution functions as they are typically observed by the Helios probes in the solar wind between 0.3 AU and 1 AU. The observational results have been compared with predictions of theoretical approaches describing the propagation of electrons in the solar wind.

The salient features of the electron distribution functions may be summarized as follows:

1. The most obvious differences for different electron distribution functions are observed at larger energies, typically above 50 eV or 100 eV. (1) We have considered a distribution function with a "narrow" strahl, which is extremely anisotropic and skewed with respect to the magnetic field direction at particle energies above 100 eV. For this distribution function the angular width of the strahl decreases with particle energy, varying typically from 20° at about 100 eV to less than 5° above 600 eV. The number of halo electrons moving along the magnetic field away from the sun is typically two or three orders of magnitude larger than the number of electrons of the same energy moving toward the sun. (2) We also have discussed a distribution function with a broad strahl which is less anisotropic and less skewed. For this distribution function the angular width of the strahl is increased at all energies in the halo regime and decreases only slowly with particle energy. For example, the angular width is typically 40° at an energy of 100 eV and decreases to 30° for energies above 400 eV. The number of halo electrons moving along the magnetic field away from the sun is typically one or two orders of magnitude larger than the number of electrons with the same energy moving toward the sun. We have concluded that here the effective collision frequency for scattering of halo electrons has increased for all energies in the energy regime of the halo up to several hundred eV, although these scattering processes do not necessarily have to occur locally. We could not determine the nature of the scattering processes. However, processes with a collision frequency strongly decreasing with particle energy such as Coulomb collisions do not seem to be the dominant scattering mechanism for halo electrons. (3) Finally, we have considered also a distribution function which has been nearly isotropic at all energies but showing a slight bidirectional anisotropy. Here scattering of halo electrons should be most effective, possibly due to a strongly increased effective collision frequency for microscopic scattering processes and/or due to trapping of the electrons in closed magnetic field loops being carried outward by the solar wind.

2. For each distribution function the phase space density decreases monotonically with energy. A break in the slope separating the core from the halo may be discerned for velocity directions along the magnetic field toward the sun and perpendicular to the magnetic field in the case of the anisotropic distribution functions. For the isotropic distribution function such a break occurs for all velocity directions. The observations have been interpreted to indicate that for anisotropic distribution functions the break in the slopes may be determined by the combined action of the interplanetary electrostatic potential and scattering processes, whereas for the nearly isotropic distribution function the break could be caused predominantly by scattering processes. However, the relative importance of both mechanisms and possibly of other effects as well as the nature of scattering processes has still to be clarified.

Representation of the distribution functions by a superposition of two bi-Maxwellian fits (the core fit and the halo fit) may be a rough description of the average thermal electron properties. However, it does not reproduce details of the distribution functions which may be important for more refined theories of electron propagation and in particular for the analysis of various microinstabilities.

3. The shift between the core peak and the solar wind bulk velocity is drastically reduced as compared to the shift predicted by exospheric theory. In the case of the anisotropic distribution functions it has not become clear whether Coulomb collisions between core electrons and protons are the only interaction mechanism to provide this reduction for the shift. In the case of the isotropic distribution function this shift is probably not significantly different from zero and may be determined by trapping of the electrons in closed magnetic field strucures.

4. For the anisotropic distribution functions the strahl carries the major part of the heat flux. For the nearly isotropic distribution function the heat flux does not seem to be significantly different from zero. Here most of the heat flux is carried by the core electrons, and the more energetic halo electrons carry even a negative heat flux, i.e., a heat flux in opposite direction.

5. The pitch angle distributions of the more energetic electrons may provide some indications for the global structure of the interplanetary magnetic field. Insofar as the pitch angle distributions are extremely asymmetric, where most of the electrons move away from the sun with small pitch angles, the magnetic field lines should reach from the solar surface outward to distances far beyond the position of the spacecraft. Nevertheless, the magnetic field lines may form extended loops also in this case. In fact, for the distribution function with the narrow strahl, a slight second peak has been seen in the pitch angle distributions at the velocity direction of backstreaming electrons at all energies (see Table 1). This may have been caused by electrons having been guided back toward the sun by extended magnetic field loops [see also *Pilipp et al.*, this issue (*a*, *b*)]. In case of magnetic field loops reaching from the sun only up to the distance of the spacecraft, or of magnetic field loops being disconnected from the sun with scale sizes not much larger than the distance from the sun, we expect to observe about as many electrons traveling toward the sun as electrons traveling outward (i.e., we expect symmetric pitch angle distributions), since the particle velocities of the electrons are much larger than the solar wind bulk velocity. The slight bidirectional anisotropy observed in the pitch angle distributions of the nearly isotropic distribution function may be an indication for such magnetic field loops, although different processes causing such pitch angle distributions cannot be excluded [e.g., *Ogilvie and Scudder*, 1981].

Acknowledgments. One of us (W. Pilipp) thanks C. T. Dum, E. Marsch and J. Scudder for helpful discussions. A careful reading of a preliminary version of the manuscript by E. Marsch resulting in valuable comments is gratefully acknowledged. We also thank F. Neubauer and his coworkers for making their magnetic field data available for this study. The Helios project is jointly conducted and supported by the German Bundesministerium für Forschung und Technologie (BMFT) and the U.S. National Aeronautics and Space Administration (NASA). The Helios plasma experiment and its data evaluation and scientific interpretation are supported by the BMFT under grants WRS 10/7 and WRS 0108.

The Editor thanks W. C. Feldman and J. D. Scudder for their assistance in evaluating this paper.

REFERENCES

Bame, S. J., J. R. Asbridge, W. C. Feldman, J. T. Gosling, and R. D. Zwickl, Bidirectional streaming of solar wind electrons >80 eV: ISEE evidence for a closed-field structure within the driver gas of an interplanetary shock, *Geophys. Res. Lett.*, *8*, 173, 1981.

Dum, C. T., E. Marsch, and W. Pilipp, Determination of wave growth from measured distribution functions and transport theory, *J. Plasma Phys.*, *23*, 91, 1980.

Feldman, W. C., J. R. Asbridge, S. J. Bame, and M. D. Montgomery, Solar wind heat transport in the vicinity of the earth's bow shock, *J. Geophys. Res.*, *78*, 3697, 1973.

Feldman, W. C., M. D. Montgomery, J. R. Asbridge, S. J. Bame, and H. R. Lewis, Interplanetary heat conduction—Imp 7 results, in *Solar Wind Three*, edited by C. T. Russell, p. 334, Institute of Geophysics and Planetary Physics, University of California, Los Angeles, 1974.

Feldman, W. C., J. R. Asbridge, S. J. Bame, M. D. Montgomery, and S. P. Gary, Solar wind electrons, *J. Geophys. Res.*, *80*, 4181, 1975.

Feldman, W. C., J. R. Asbridge, S. J. Bame, S. P. Gary, and M. D. Montgomery, Electron parameter correlations in high-speed streams and heat flux instabilities, *J. Geophys. Res.*, *81*, 2377, 1976*a*.

Feldman, W. C., J. R. Asbridge, S. J. Bame, S. P. Gary, M. D. Montgomery, and S. M. Zink, Evidence for the regulation of solar wind heat flux at 1 AU, *J. Geophys. Res.*, *81*, 5207, 1976*b*.

Feldman, W. C., J. R. Asbridge, S. J. Bame, J. T. Gosling, and D. S. Lemons, Characteristic electron variations across simple high-speed solar wind streams, *J. Geophys. Res.*, *83*, 5285, 1978.

Feldman, W. C., J. R. Asbridge, S. J. Bame, J. T. Gosling, and D. S. Lemons, The core electron temperature profile between 0.5 and 1.0 AU in the steady-state high speed solar wind, *J. Geophys. Res.*, *84*, 4463, 1979*a*.

Feldman, W. C., J. R. Asbridge, S. J. Bame, J. T. Gosling, and D. S. Lemons, A possible closure relation for heat transport in the solar wind, *J. Geophys. Res.*, *84*, 6621, 1979*b*.

Feldman, W. C., J. R. Asbridge, S. J. Bame, and J. T. Gosling, Quantitative tests of a steady state theory of solar wind electrons, *J. Geophys. Res.*, *87*, 7355, 1982.

Formisano, V., Interplanetary plasma electrons: A preliminary report of Pioneer 6 data, *J. Geophys. Res.*, *74*, 355, 1969.

Gurnett, D. A., and R. R. Anderson, Plasma wave electric fields in the solar wind: Initial results from Helios 1, *J. Geophys. Res.*, *82*, 632,1977.

Hollweg, J. V., On electron heat conduction in the solar wind, *J. Geophys. Res.*, *79*, 3845, 1974.

Hollweg, J. V., Collisionless electron heat conduction in the solar wind, *J. Geophys. Res.*, *81*, 1649, 1976.

Isensee, U., Plasma disturbances caused by the Helios spacecraft in the solar wind, *J. Geophys.*, *42*, 581, 1977.

Isensee, U., and H. Maassberg, Particle-in-cell simulation of the plasma environment of a spacecraft in the solar wind, *Adv. Space Res.*, *1*, 413, 1981.

Jockers, K., Solar wind models based on exospheric theory, *Astron. Astrophys.*, *6*, 219, 1970.

Lemaire, J., and M. Scherer, Kinetic models of the solar wind, *J. Geophys. Res.*, *76*, 7479, 1971.

Lemons, D. S., and W. C. Feldman, Collisional modification to the exospheric theory of solar wind halo electron pitch angle distributions, *J. Geophys. Res.*, *88*, 6881, 1983.

Maassberg, H., and U. Isensee, Symmetric theory of probe-plasma interactions, *Planet. Space Sci.*, *29*, 555, 1981.

Marsch, E., K.-H. Mühlhäuser, R. Schwenn, H. Rosenbauer, W. Pilipp, and F. M. Neubauer, Solar wind protons: Three-dimensional velocity distributions and derived plasma parameters measured between 0.3 and 1 AU, *J. Geophys. Res.*, *87*, 52, 1982*a*.

Marsch, E., K.-H. Mühlhäuser, H. Rosenbauer, R. Schwenn, and F. M. Neubauer, Solar wind helium ions: Observations of the Helios solar probes between 0.3 and 1 AU, *J. Geophys. Res.*, *87*, 35, 1982*b*.

Montgomery, M. D., Average thermal characteristics of solar wind electrons, in Solar Wind, edited by C. P. Sonett, P. J. Coleman, Jr., and J. M. Wilcox, *NASA Spec. Publ.*, *SP-308*, 208, 1972*a*.

Montgomery, M. D.,Thermal energy transport in the solar wind, in *Cosmic Plasma Physics*, edited by K. Schindler, p. 61, Plenum, New York, 1972*b*.

Montgomery, M. D., S. J. Bame, and A. J. Hundhausen, Solar wind electrons: Vela 4 measurements, *J. Geophys. Res.*, *73*, 4999, 1968.

Montgomery, M. D., J. R. Asbridge, S. J. Bame, and W. C. Feldman, Solar wind electron temperature depressions following

some interplanetary shock waves: Evidence for magnetic merging?, *J. Geophys. Res.*, *79*, 3103, 1974.

Musmann, G., F. M. Neubauer, A. Maier, and E. H. Lammers, Das Förstersonden-Magnetfeldexperiment (E2), *Raumfahrtforschung*, *19*, 232, 1975.

Musmann, G., F. M. Neubauer, and E. Lammers, Radial variation of the interplanetary magnetic field between 0.3 AU and 1.0 AU, *J. Geophys.*, *42*, 591, 1977.

Neubauer, F. M., G. Musmann, and G. Dehmel, Fast magnetic fluctuations in the solar wind: Helios 1, *J. Geophys. Res.*, *82*, 3201, 1977.

Ogilvie, K. W., and J. D. Scudder, The radial gradient and collisionless properties of solar wind electrons, *J. Geophys. Res.*, *83*, 3776, 1978.

Ogilvie, K. W., and J. D. Scudder, Observations of the 'Strahl' by the solar wind electron spectrometer on Mariner 10, in Solar Wind Four, *Rep. MPAE-W-100-81-31*, edited by H. Rosenbauer, p. 250, Max-Planck-Inst. für Aeron., Katlenburg-Lindau, West Germany, 1981.

Ogilvie, K. W., J. D. Scudder, and M. Sugiura, Electron energy flux in the solar wind, *J. Geophys. Res.*, *76*, 8165, 1971.

Olbert. S., Role of thermal conduction in the acceleration of the solar wind, in Solar Wind Five, edited by M. Neugebauer, *NASA Conf. Publ.*, *2280*, 149, 1983.

Perkins, F., Heat conductivity, plasma instabilities, and radio star scintillations in the solar wind, *Astrophys. J.*, *179*, 637, 1973.

Pilipp, W. G., Solar wind electrons as a probe for the global structure of the interplanetary magnetic field, in *Topics in Plasma-, Astro- and Space Physics*, edited by G. Haerendel and B. Battrick, p. 91, Max-Planck-Institut für Physik und Astrophysik, Institut für extraterrestrische. Physik, Garching bei München, West Germany, 1983.

Pilipp, W. G., R. Schwenn, E. Marsch, K.-H.Mühlhäuser, and H. Rosenbauer, Electron characteristics in the solar wind as deduced from Helios observations, in Solar Wind Four, *Rep. MPAE-W-100-81-31*, edited by H. Rosenbauer, p. 241, Max-Planck-Inst. für Aeron., Katlenburg-Lindau, West Germany, 1981.

Pilipp, W. G., H. Miggenrieder, K.-H. Mühlhäuser, H. Rosenbauer,and R. Schwenn, Data analysis of electron measurements of the plasma experiment aboard the Helios probes, *MPE Rep. 185*, Max-Planck-Inst. für Phys. und Astrophys. Inst. für extraterr. Phys., Garching bei München, West Germany, 1984.

Pilipp, W. G., H. Miggenrieder, M. D. Montgomery, K.-H. Mühlhäuser, H. Rosenbauer, and R. Schwenn, Unusual electron distribution functions in the solar wind derived from the Helios plasma experiment: Double-strahl distributions and distributions with an extremely anisotropic core, *J. Geophys. Res.*, this issue (*a*).

Pilipp, W. G., H. Miggenrieder, K.-H. Mühlhäuser, H. Rosenbauer, R. Schwenn, and F. M. Neubauer, Variations of electron distribution functions in the solar wind, *J. Geophys. Res.*, this issue (*b*).

Porsche, H., Die Helios-Sonde als Experimententräger, *Raumfahrtforschung*, *19*, 223, 1975.

Porsche, H., General aspects of the mission Helios 1 and 2, *J. Geophys.*, *42*, 551, 1977.

Rosenbauer, H., Possible effects of the photo electron emission on a low energy electron experiment, in *Photon and Particle Interactions with Surfaces in Space*, edited by R. J. L. Grard, p. 139, D. Reidel, Hingham, Mass., 1973.

Rosenbauer, H., H. Miggenrieder, M. Montgomery, and R. Schwenn, Preliminary results of the Helios plasma measurements, in *Physics of Solar Planetary Environments*, edited by D. J. Williams, p. 319, AGU, Washington, D. C., 1976.

Rosenbauer, H., R. Schwenn, E. Marsch, B. Meyer, H. Miggenrieder, M. D. Montgomery, K.-H. Mühlhäuser, W. Pilipp, W. Voges, and S. M. Zink, A survey on initial results of the Helios plasma experiment, *J. Geophys.*, *42*, 561, 1977.

Rosenbauer, H., R. Schwenn, H. Miggenrieder, B. Meyer, H. Grünwaldt, K.-H. Mühlhäuser, H. Pellkofer, and J. H. Wolfe, Die Instrumente des Plasmaexperiments auf den Helios-Sonnensonden, *Rep. BMFT-FB-W 81-015*, Max-Planck-Inst. für Aeron., Katlenburg-Lindau, West Germany, 1981.

Schulz, M., and A. Eviatar, Electron-temperature asymmetry and the structure of the solar wind, *Cosmic Electrodyn.*, *2*, 402, 1972.

Schwenn, R., H. Rosenbauer, and H. Miggenrieder, Das Plasmaexperiment auf Helios (E1), *Raumfahrtforschung*, *19*, 226, 1975.

Scudder, J. D., Comments, in Solar Wind, edited by C. P. Sonett, P. J. Coleman, Jr., and J. M. Wilcox, *NASA Spec. Publ.*, *SP-308*, 211, 1972.

Scudder, J. D., and S. Olbert, A theory of local and global processes which affect solar wind electrons, 1, The origin of typical 1 AU velocity distribution functions: Steady state theory, *J. Geophys. Res.*, *84*, 2755, 1979*a*.

Scudder, J. D., and S. Olbert, A theory of local and global processes which affect solar wind electrons, 2, Experimental support, *J. Geophys. Res.*, *84*, 6603, 1979*b*.

Scudder, J. D., D. L. Lind, and K. W. Ogilvie, Electron observations in the solar wind and magnetosheath, *J. Geophys. Res.*, *78*, 6535, 1973.

Serbu, G. P., Explorer 35 observations of solar wind electron density, temperature, and anisotropy, *J. Geophys. Res.*, *77*, 1703, 1972.

Sheeley, N. R., Jr., and J. W. Harvey, Coronal holes, solar wind streams, and geomagnetic activity during the new sunspot cycle, *Sol. Phys.*, *59*, 159, 1978.

Sittler, E. C., Jr., and J. D. Scudder, An empirical polytrope law for solar wind thermal electrons between 0.45 and 4.76 AU: Voyager 2 and Mariner 10, *J. Geophys. Res.*, *85*, 5131, 1980.

Sittler, E. C., Jr., J. D. Scudder, and J. Jessen, Radial variation of solar wind thermal electrons between 1.36 and 2.25 AU: Voyager 2, in Solar Wind Four, *Rep. MPAE-W-100-81-31*, edited by H. Rosenbauer, p. 257, Max-Planck-Inst. für Aeron., Katlenburg-Lindau, West Germany, 1981.

Spitzer, L., Jr., and R. Härm, Transport phenomena in a completely ionized gas, *Phys. Rev.*, *89*, 977, 1953.

Temnyi, V. V., and O. L. Vaisberg, A dumbbell distribution of epithermal electrons in solar wind based on observations on the Prognoz 7 satellite, *Cosmic Res.*, Engl. Transl., *17*, 476, 1979. (Translated from *Kosm. Issled.*, *17*, 580, 1979.)

Voigt, G.-H., U. Isensee, and H. Maassberg, Calculation of the disturbances of the low energy electron measurements, in Helios Solar Probes Science Summaries, *NASA Tech. Memo.*, *TM-82005*, 12, 1980.

Voigt, G.-H., U. Isensee, and H. Maassberg, Die Wechselwirkungen der Helios-Sonde mit dem Plasma des solaren Windes, *Rep. BMFT-FB-W 81-036*, Tech. Hochsch. Darmstadt, Darmstadt, West Germany, 1981.

H. Miggenrieder, Bayerisches Staatsministerium für Landesentwicklung und Umweltfragen, Rosenkavalierplatz 2, 8000 München, Federal Republic of Germany.

M. D. Montgomery, Maxwell Laboratories, Inc., 8888 Balboa Avenue, San Diego, CA 92123.

K.-H. Mühlhäuser and W. G. Pilipp, Max-Planck-Institut für Physik und Astrophysik, Institut für extraterrestrische Physik, D-8046 Garching bei München, Federal Republic of Germany.

H. Rosenbauer and R. Schwenn, Max-Planck-Institut für Aeromonie, 3411 Katlenburg-Lindau, Federal Republic of Germany.

(Received May 16, 1985;
revised July 16, 1986;
accepted August 14, 1986.)